# Shell structure evolution and effective in-medium NN interaction

N. A. Smirnova

*Centre d'Etudes Nucléaires de Bordeaux Gradignan, CNRS/IN2P3 - Université Bordeaux 1, Chemin du Solarium, BP 120, 33175 Gradignan, France*

The nuclear many-body problem is considered in the framework of the shell model. In the first part, we review the formalism of the nuclear shell model: oscillator based expansion for the wave function, diagonalization of the residual interaction, types of the effective interactions used in the calculations. In the second part, a multipole decomposition of the shell-model Hamiltonian is introduced. The monopole part of the Hamiltonian governs the spherical nuclear mean field and defines shell gaps, while the higher multipole part contains particle-particle correlations. The mechanism for the formation or disappearance of different magic numbers is outlined (competition between closed-shell configurations and intruder configurations). Variations of spherical single-particle energies in series of isotopes or isotones, as obtained by realistic interactions, are explored in a few regions of nuclear chart. The role of different components of the effective NN interaction is discussed in terms of schematic forces and is further elucidated by the spin-tensor decomposition of the two-body matrix elements in the $(1s0d1p0f)$ shell-model space.

# Contents

# 1 Introduction

The shell model represents a powerful tool in nuclear structure. If the model space contains all physically relevant degrees of freedom and the residual interaction is well adjusted, the shell model describes nuclear spectra at low energies and transition probabilities rather accurately. The oscillator-based expansion for the wave function allows to analyze the structure of the states in terms of different configurations. It is also very instructive to consider specific cases of schematic interactions when sometimes an analytically solvable Hamiltonian can describe well a part of an experimental spectrum and transition rates, and therefore shed light on the nature of the states.

The purpose of these lectures is first to revise the basic ideas behind the nuclear shell model. In particular, we consider in simple examples how to construct a basis from single-particle solutions, how to solve a many-particle problem by diagonalization of the Hamiltonian matrix and how to choose or construct an effective interaction.

The shell model is then applied to explore the evolution of the shell structure in nuclei far from stability. We will be interested in the mechanism responsible for the weakening of shell closures, characteristic for nuclei close to the valley of β-stability. In particular, we will study variations of spherical single-particle energies and associated spherical shell gaps in series of isotopes or isotones. Finally, we will focus on the role of different terms of the effective nucleon-nucleon (NN) interaction in the shell evolution.

# 2 Basic principles of the nuclear shell model

The basic assumption of the nuclear shell model is that to a first approximation each nucleon moves independently in a potential that represents the average interaction with the other nucleons in a nucleus. This independent motion can be understood qualitatively from a combination of the weakness of the long-range nuclear attraction and the Pauli exclusion principle.

In a non-relativistic approximation, nuclear properties are described by the Schrödinger equation for $A$ nucleons

$$\hat{H}\Psi(1,2,\ldots,A) = E\Psi(1,2,\ldots,A)\,, \tag{1}$$

where $\hat{H}$ contains nucleon kinetic energy operators and interactions between nucleons — of a two-body and, eventually, of a three-body character, i.e.

$$\hat{H} = \sum_{i=1}^{A} \left( -\frac{\hbar^2}{2m} \Delta_i \right) + \sum_{i<j=1}^{A} W(i,j) + \sum_{i<j<k=1}^{A} W(i,j,k) \,, \tag{2}$$

$\Psi(1,2,\ldots,A)$ is an $A$-body wave function, while $i$ denotes all relevant coordinates $\vec{r}_i, \vec{s}_i, \vec{t}_i$ of a given particle ($i = 1,2,\ldots,A$). Although the three-body forces are proved to be important [57, 56, 46], in the present course we will consider only the two-body interaction.

We can re-write the Hamiltonian (2), adding and subtracting a one-body potential of the form $\sum_{i=1}^{A} U(i)$ as

$$\hat{H} = \sum_{i=1}^{A} \left[ -\frac{\hbar^2}{2m} \Delta_i + U(i) \right] + \sum_{i<j=1}^{A} W(i,j) - \sum_{i=1}^{A} U(i) = \hat{H}^{(0)} + \hat{V} \,, \tag{3}$$

where we denoted a sum of single-particle Hamiltonians as $\hat{H}^{(0)}$,

$$\hat{H}^{(0)} = \sum_{i=1}^{A} \left[ -\frac{\hbar^2}{2m} \Delta_i + U(i) \right] \equiv \sum_{i=1}^{A} \hat{h}(i) \,, \tag{4}$$

and $\hat{V}$ is called a *residual interaction*. Existence of a nuclear average potential allows to assume that we can find such a potential $\sum_{i=1}^{A} U(i)$, that the residual interaction $V$ is small.

One way to obtain the most optimal mean-field potential is provided in the framework of the *Hartree-Fock theory*. Given a two-body interaction with typically global parametrization, one aims at deriving the best mean-field potential by minimizing the total energy of the system. Then one searches how to account for correlations beyond the mean-field approximation (see lecture of M. Grasso in this volume).

The nuclear shell model follows another strategy. $U(i)$ is chosen to be a known suitable potential (e.g., the harmonic oscillator potential, or the Woods-Saxon potential, or the square-well). Solutions of a single-particle problem for $\hat{h}$ with this potential are used to construct a basis for further diagonalization of the residual interaction $\hat{V}$.

The full theory of the nuclear shell model can be found in numerous excellent books (e.g. [17, 32]), only main principles will be presented here in a few first sections as an introduction to the second part. In section 3 we revise a single-particle problem with the harmonic oscillator potential. Section 4 is devoted to the basis contruction and diagonalization problem. In section 5 we discuss different types of effective interactions, including microscopic ones. In section 6 we re-write the shell-model Hamiltonian in a second quantization formalism and we perform a separation into multipole parts. Sections 7 and 8 are devoted to the description of exotic nuclei and shell evolution far from stability. The modern status of the shell model and various applications to nuclear spectroscopy, including structure exotic nuclei, can be found in reviews [54, 12, 18]. Two courses on the shell model, covering some of the topics discussed here, have been previously given at Joliot-Curie School by A. Poves [58] and F. Nowacki [47].

# 3 Single-particle wave functions

## 3.1 Particle in a spherically symmetric potential

Solutions of a single-particle problem serve to construct a basis to diagonalize the residual shell-model interaction. To start with, let us revise the solution of the eigenproblem for a particle in a spherically symmetric potential $U(\vec{r}) \equiv U(r)$. Then the Schrödinger equation

$$\hat{h}\phi(\vec{r}) \equiv \left(-\frac{\hbar^2}{2m}\Delta + U(r)\right)\phi(\vec{r}) = \varepsilon\phi(\vec{r}) \tag{5}$$

is separable in radial and angular coordinates. The eigenfunctions can be expressed as

$$\phi_{nlm_l}(\vec{r}) = \frac{R_{nl}(r)}{r} Y_{lm_l}(\theta,\varphi)\,, \tag{6}$$

where $Y_{lm_l}(\theta,\varphi)$ are spherical harmonics, the eigenfunctions of the squared orbital angular momentum operator and its projection on $z$-axis:

$$\begin{aligned} \hat{l}^2 Y_{lm_l}(\theta,\varphi) &= l(l+1)Y_{lm_l}(\theta,\varphi)\,, \\ \hat{l}_z Y_{lm_l}(\theta,\varphi) &= m_l Y_{lm_l}(\theta,\varphi)\,. \end{aligned} \tag{7}$$

The radial part, denoted as $R_{nl}(r)$, is solution of the one-dimensional second-order differential equation

$$-\frac{\hbar^2}{2m}R''(r) + \frac{\hbar^2}{2m}\frac{l(l+1)}{r^2}R(r) + U(r)R(r) = \varepsilon R(r)\,. \tag{8}$$

We will use here the radial quantum number $n = 0,1,2,3,\ldots$ to label different solutions of this equation (number of zeros of R(r)). Single-particle wave functions transform under a parity operation $\hat{P}(\vec{r}) \to (-\vec{r})$ following the rule:

$$\hat{P}\left(\phi_{nlm_l}(\vec{r})\right) = \hat{P}\left(\frac{R_{nl}(r)}{r}Y_{lm_l}(\theta,\varphi)\right) = \frac{R_{nl}(r)}{r}(-1)^l Y_{lm_l}(\theta,\varphi) = (-1)^l \phi_{nlm_l}(\vec{r})\,. \tag{9}$$

For a particle with an intrinsic spin we must consider the spin-orbit interaction. The corresponding Schrödinger equation reads

$$-\frac{\hbar^2}{2m}\Delta\phi(\vec{r}) + U(r)\phi(\vec{r}) + f_{ls}(r)(\vec{l}\cdot\vec{s})\phi(\vec{r}) = \varepsilon\phi(\vec{r})\,. \tag{10}$$

The single-particle wave function of a particle with an intrinsic spin $1/2$ takes then a form

$$\phi_{nlsjm}(\vec{r},\vec{s}) = \frac{R_{nlj}(r)}{r}\left[Y_l(\theta,\varphi)\times\chi_{\frac{1}{2}}(\vec{s})\right]^{(j)}_m = \frac{R_{nlj}(r)}{r}\sum_{m_l m_s}(lm_l\tfrac{1}{2}m_s|jm)Y_{lm_l}(\theta,\varphi)\chi_{\frac{1}{2}m_s}\,, \tag{11}$$

where $\chi_{\frac{1}{2}m_s}$ denotes a spin-$1/2$ spinor, $j$ is the quantum number associated with the total angular momentum operator $\vec{j} = \vec{l} + \vec{s}$ which is conserved, and the coefficients in the round brackets are the Clebsch-Gordan coefficients. The radial wave functions become solutions of the following second-order differential equation:

$$-\frac{\hbar^2}{2m}R''(r) + \frac{\hbar^2}{2m}\frac{l(l+1)}{r^2}R(r) + \left[U(r)R(r) + a_{ls}f_{ls}(r)\right]R(r) = \varepsilon R(r), \tag{12}$$

with $a_{ls}$ being eigenvalues of the $(\vec{l}\cdot\vec{s})$ operator in a state with definite $l$, $s$ and $j$ quantum number.
`Exercise. Calculate` $a_{ls}$ `for a state characterized by` $nlj$ `quantum numbers.`
For finite potentials, eq. (12) has both discrete solutions, corresponding to bound states ($\varepsilon < 0$), and continuum solutions ($\varepsilon > 0$). Bound states are normalized according to a condition:

$$\begin{aligned}\int |\phi_{nlsjm}(\vec{r},\vec{s})|^2 d\vec{r} &= \sum_{m_l,m_s,m_l',m_s'} (lm_l\tfrac{1}{2}m_s|jm)(lm_l'\tfrac{1}{2}m_s'|jm)\int Y_{lm_l}(\theta,\varphi)Y_{lm_l'}(\theta,\varphi)d\Omega \\ &\times \langle\chi_{\frac{1}{2}m_s}|\chi_{\frac{1}{2}m_s'}\rangle \int_0^\infty |R_{nl}(r)|^2 dr = \int_0^\infty |R_{nl}(r)|^2 dr = 1\end{aligned} \tag{13}$$

## 3.2 Harmonic oscillator potential

The explicit form of the radial part will depend on the spherically symmetric potential considered. The choice of the potential will influence the efficiency of the solution of a many-body problem. Let us suppose that each nucleon moves in a harmonic oscillator potential:

$$U(r) = \frac{m\omega^2 r^2}{2}\,. \tag{14}$$

The solution of eq. (8) with the harmonic oscillator potential have a form:

$$R_{nl}(r) = N_{nl}\, r^{l+1} \exp\left(-\frac{r^2}{2b^2}\right) L_n^{l+1/2}\left(\frac{r^2}{b^2}\right)\,, \tag{15}$$

where $b = \sqrt{\frac{\hbar}{m\omega}}$ is the harmonic oscillator length parameter and $L_n^{l+1/2}\left(\frac{r^2}{b^2}\right)$ are generalized Laguerre polynomials. The normalization factor $N_{nl}$ is defined by the condition

$$\int_0^\infty R_{nl}^2(r)dr = 1\,. \tag{16}$$

The energy eigenvalues are given by

$$\varepsilon_N = \hbar\omega\left(2n+l+\frac{3}{2}\right) = \hbar\omega\left(N+\frac{3}{2}\right)\,, \tag{17}$$

with

$$\begin{aligned} &N = 0,1,2,\ldots, \\ &l = N, N-2, \ldots, 1 \text{ or } 0 \\ &n = (N-l)/2\,. \end{aligned} \tag{18}$$

The energy level with a given $N$ is called an *oscillator shell*. The states corresponding to different $n$ and $l$ values can be labeled as shown in Table 1 (here the numbers refer to the values of $n$ and the letters $s,p,d,f,g,\ldots$ denote states with $l = 0,1,2,3,4,\ldots$, respectively). The equidistant energy spectrum is shown in Fig. 1 (left).

Each oscillator shell contains orbitals with either even or odd values of $l$ and hence it is either even or odd with respect to the parity operation (9). The total degeneracy of the $N$th oscillator shell for identical spin $1/2$ nucleons is

$$\Omega_N = \sum_{l=0\,\text{or}\,1}^{N} 2(2l+1) = (N+1)(N+2)\,, \tag{19}$$

Table 1: Notations of single-particle states in the harmonic oscillator potential.

| $N=0$ | $N=1$ | $N=2$ | $N=3$ | $N=4$ | $N=5$ | ... |
|---|---|---|---|---|---|---|
| $0s$ | $0p$ | $0d$, $1s$ | $0f$, $1p$ | $0g$, $1d$, $2s$ | $0h$, $1f$, $2p$ | ... |

The distance between two different shells is estimated as

$$\hbar\omega = 41A^{-1/3}\mathrm{MeV}\,. \tag{20}$$

The degeneracy of the oscillator shell can be removed by addition of a centrifugal term $(\vec{l}\cdot\vec{l})$ and a spin-orbit coupling term $(\vec{l}\cdot\vec{s})$:

$$\hat{h} = -\frac{\hbar^2}{2m}\Delta + \frac{m\omega^2 r^2}{2} + f_{ll}(r)(\vec{l}\cdot\vec{l}) + f_{ls}(r)(\vec{l}\cdot\vec{s})\,. \tag{21}$$

The centrifugal term separates states having the same $N$, but different $l$ quantum numbers as shown in Fig. 1 (center). Spin-orbit splitting leads to appearance of the states characterized by different values of the total angular momentum $j = l \pm 1/2$, see Fig. 1 (right). The single-particle wave function has thus a form of eq.(11).

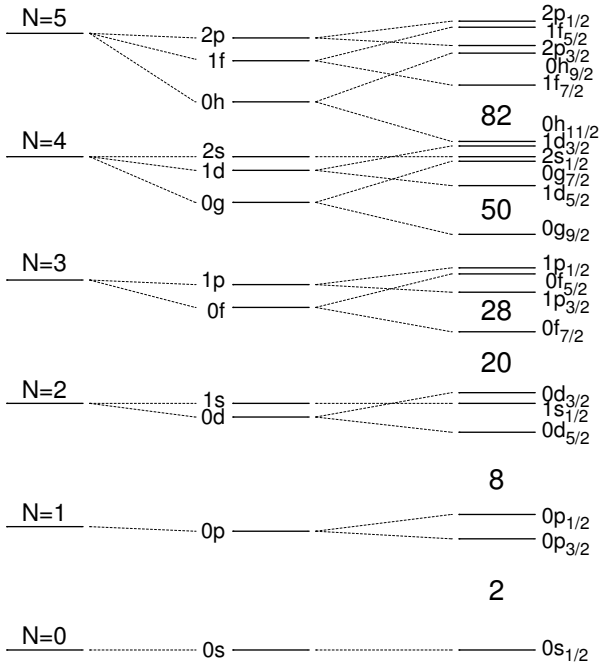


Figure 1: Single-particle level schemes obtained with (i) a harmonic-oscillator potential (14) (left), (ii) harmonic-oscillator potential plus a centrifugal term (center), (iii) harmonic-oscillator potential plus both a centrifugal term and a spin-orbit term (right).

## 3.3 Isospin

As is well known, the interaction between two protons (Coulomb interaction subtracted), two neutrons or a proton and a neutron is approximately the same, i.e. $v_{\pi\pi} \approx v_{\nu\nu} \approx v_{\pi\nu}$. It was an idea of Heisenberg to introduce a new quantum number, *isospin*, to distinguish between two types of nucleons. Similarly to the intrinsic spin, nucleons are considered to carry an isospin $t = 1/2$, with neutrons being characterized by its projection $m_t = 1/2$ and protons being characterized by $m_t = -1/2$. Single-particle wave functions of a neutron and a proton can be expressed with the help of $t = 1/2$ spinors as

$$\begin{aligned} \phi_\nu(r) &= \phi(\vec{r}) \begin{pmatrix} 1 \\ 0 \end{pmatrix} = \phi(\vec{r})\, \theta_{t=1/2, m_t=1/2}\,, \\ \phi_\pi(r) &= \phi(\vec{r}) \begin{pmatrix} 0 \\ 1 \end{pmatrix} = \phi(\vec{r})\, \theta_{t=1/2, m_t=-1/2}\,. \end{aligned} \tag{22}$$

Similarly to the angular momentum, we can introduce an isospin operator, a vector $\vec{t} = \frac{1}{2}\vec{\tau}$, where three components of the vector $\vec{\tau}$ have a form of the Pauli matrices:

$$\tau_x = \begin{pmatrix} 0 & 1 \\ 1 & 0 \end{pmatrix}, \quad \tau_y = \begin{pmatrix} 0 & -i \\ i & 0 \end{pmatrix}, \quad \tau_z = \begin{pmatrix} 1 & 0 \\ 0 & -1 \end{pmatrix} \tag{23}$$

The ladder operators, $t_\pm = \frac{1}{2}(\tau_x \pm i\tau_y)$, thus convert a proton into a neutron and vice versa:

$$\begin{aligned} t_+\phi_\pi(\vec{r}) &= \phi_\nu(\vec{r})\,, & t_-\phi_\pi(\vec{r}) &= 0 \\ t_+\phi_\nu(\vec{r}) &= 0\,, & t_-\phi_\nu(\vec{r}) &= \phi_\pi(\vec{r}) \end{aligned} \tag{24}$$

Thus the full explicit form of a single-nucleon wave function reads

$$\phi_{nlsjm,tm_t}(\vec{r},\vec{s},\vec{t}) = R_{nl}(r)\left[Y_l(\theta,\varphi) \times \chi_{1/2}(\vec{s})\right]^{(j)}_m \theta_{1/2}(\vec{t})\,. \tag{25}$$

The wave function (25) is a coordinate-spin-isospin representation of a state vector $|nlsjm, tm_t\rangle$:

$$\langle \vec{r}, \vec{s}, \vec{t}\,|nlsjm; tm_t\rangle \equiv \phi_{nlsjm,tm_t}(\vec{r},\vec{s},\vec{t}) \tag{26}$$

Isospin operators can be used similarly to the angular momentum operators to construct isospin states of a many-nucleon system:

$$\hat{T} = \sum_{i=1}^{A} \hat{t}_i, \quad \hat{T}_z = \sum_{i=1}^{A} \hat{t}_{zi}\,. \tag{27}$$

Charge independence of a nuclear interaction thus leads to a new symmetry, called an *isospin symmetry*. If the Hamiltonian is charge independent, i.e. if it commutes with the total isospin operator $\hat{T}$,

$$\left[\hat{H}, \hat{T}\right] = 0\,. \tag{28}$$

then the nuclear states of a nucleus with $N$ neutrons and $Z$ protons ($A = N+Z$) can be characterized by definite values of $T$ and $M_T$ quantum numbers:

$$M_T = \frac{1}{2}(N-Z), \quad \frac{1}{2}(N-Z) \le T \le \frac{A}{2}\,. \tag{29}$$

Isospin quantum number represents a convenient way to deal with nucleon wave functions and it is valid when the nuclear Hamiltonian under consideration does not break the isospin symmetry (electromagnetic interactions are not considered). An alternative possibility is to label explicitly nucleon wave function by proton or neutron indices which will lead to equivalent results.

The addition of the Coulomb interaction between protons will break the isospin symmetry. Since the effect is small, for many purposes it can be accounted within the perturbation theory. The Coulomb interaction can be expressed in the isospin formalism as a following sum over valence protons

$$\hat{V}_{Coulomb} = \sum_{i<j} \left[\frac{1}{2} + \hat{t}_z(i)\right] \left[\frac{1}{2} + \hat{t}_z(j)\right] \frac{e^2}{r} \,. \tag{30}$$

and therefore, represents a sum of ranks $k = 0, 1, 2$ tensors in isospace:

$$\hat{V}_{Coulomb} = \hat{V}^{(T=0)} + \hat{V}^{(T=1)} + \hat{V}^{(T=2)} \,. \tag{31}$$

Thus, the nuclear states can still be characterized by the total isospin quantum number $T$, however, the states of an isospin multiplet are splitted according to the rule

$$E(T, T_z) = a(T) + b(T) M_T + c(T) M_T^2 \,, \tag{32}$$

known as the isobaric multiplet mass equation (see Refs. [71, 36, 11] for more details).

`Exercise. Starting from the expression (30) get eq. (32).`

# 4 Solution of the eigenproblem

Single-particle wave functions are used to construct many-body states which will serve as a basis to diagonalize the residual interaction. The following two methods to construct basis states are most frequently used in practical calculations.

## 4.1 $m$-scheme basis

An efficient way to construct a basis numerically is provided by the so-called $m$-scheme. The basic blocks are Slater determinants — normalized and antisymmetrized products of $A$ single-particle wave functions occupying $A$ different states:

$$\Phi_\alpha(1,2,\ldots,A) \equiv \Phi_{\alpha_1\alpha_2\ldots\alpha_A}(1,2,\ldots,A) = \frac{1}{\sqrt{A!}} \begin{vmatrix} \phi_{\alpha_1}(\vec{r}_1) & \phi_{\alpha_1}(\vec{r}_2) & \ldots & \phi_{\alpha_1}(\vec{r}_A) \\ \phi_{\alpha_2}(\vec{r}_1) & \phi_{\alpha_2}(\vec{r}_2) & \ldots & \phi_{\alpha_2}(\vec{r}_A) \\ \vdots & \vdots & \ddots & \vdots \\ \phi_{\alpha_A}(\vec{r}_1) & \phi_{\alpha_A}(\vec{r}_2) & \ldots & \phi_{\alpha_A}(\vec{r}_A) \end{vmatrix} \tag{33}$$

where $\alpha_i = (n_i, l_i, j_i, m_i)$ and $\alpha$ stores a set of single-particle configurations $\{\alpha_1, \alpha_2, \ldots, \alpha_A\}$. It is clear that the wave function (33) does not possess a certain $J$ value and only its projection $M = \sum_{i=1}^{A} m_i$ is a good quantum number.

The many-particle wave functions constructed in such a way are eigenfunctions of the Schrödinger equation for an independent particle Hamiltonian $\hat{H}^{(0)}$ (4):

$$\hat{H}^{(0)} \Phi_\alpha(1,2,\ldots,A) = E_\alpha^{(0)} \Phi_\alpha(1,2,\ldots,A) \,. \tag{34}$$

with $E_\alpha^{(0)}$ being a sum of single-particle energies from (10):

$$E_\alpha^{(0)} = \sum_{i=1}^{A} \varepsilon_{\alpha_i}\,, \tag{35}$$

All such functions in a given configuration space will form a basis. In practice, one first projects them on the states with good values of $J,T$ and then performs diagonalization of the residual interaction.

Exercise. Consider three identical nucleons in a $0f_{7/2}$ orbital. The state with the maximum $M$-value $|M=\frac{15}{2}\rangle = |m_1m_2m_3\rangle = |\frac{7}{2}\frac{5}{2}\frac{3}{2}\rangle$ corresponds to the maximum value of $J=15/2$. Distributing particles among different $m$-substates in all possible ways, find which $J$-values can be constructed.

## 4.2 $J(T)$-coupled basis

A more complicated way to get a basis of many-body states is to construct from antisymmetrized and normalized products of single-particle states linear combinations corresponding to a good angular momentum value $J$, using angular momentum algebra. The same procedure can be performed with nucleon isospin operators, coupling them to a good total isospin $T$.

Let us consider a 2-particle system. We will require a two-particle wave function to be antisymmetric with respect to interchange of all coordinates of the two nucleons and to have definite values of the total angular momentum $J$ and total isospin $T$. It is easy to verify that the wave function will have a form

$$\Phi^{ab}_{JMTM_T}(1,2) = \left\{ [\phi_a(\vec{r}_1)\times\phi_b(\vec{r}_2)]^{(J)}_M + (-1)^{j_a+j_b+J+T}\,[\phi_b(\vec{r}_1)\times\phi_a(\vec{r}_2)]^{(J)}_M \right\} \frac{\Theta_{TM_T}}{\sqrt{2(1+\delta_{ab})}}\,. \tag{36}$$

Here instead of Greek letters referring to four quantum numbers of a nucleon single-particle state ($\alpha$), we will use notation $a=(n_a l_a j_a)$ to denote three quantum labels and a separate notation for the angular momentum projection $m_a$, while $\times$ sign denotes a tensorial product of two tensor operators of ranks $j_a$ and $j_b$ which is performed by use of the Clebsch-Gordan coefficients. The total angular momentum thus takes values $J=|j_a-j_b|,|j_a-j_b|+1,\ldots,j_a+j_b$, while $M=-J,-J+1,\ldots,J-1,J$. $\Theta$ is a two-nucleon isospin part which can be expressed as

$$\begin{array}{lcl}
\Theta_{1,1} &=& \theta_{1/2,1/2}(1)\theta_{1/2,1/2}(2)\,,\\
\Theta_{1,-1} &=& \theta_{1/2,-1/2}(1)\theta_{1/2,-1/2}(2)\,,\\
\Theta_{1,0} &=& \left[\theta_{1/2,1/2}(1)\theta_{1/2,-1/2}(2)+\theta_{1/2,-1/2}(1)\theta_{1/2,1/2}(2)\right]/\sqrt{2}\,,\\
\Theta_{0,0} &=& \left[\theta_{1/2,1/2}(1)\theta_{1/2,-1/2}(2)-\theta_{1/2,-1/2}(1)\theta_{1/2,1/2}(2)\right]/\sqrt{2}\,,
\end{array} \tag{37}$$

where the Clebsch-Gordan coefficients in isospace are written explicitly.

We will remark an important case when $j_a=j_b=j$. Due to the antisymmetry, the total wave function exists only when $(J+T)$ is odd. This means that for two identical nucleons on the same $j$-shell, the total $J$ can take only even values $J=0,2,\ldots,2j-1$.

Similarly, a many-particle wave function can be constructed. For $N_a$ particles in $a$ state coupled to $J_a$ angular momentum, $N_b$ particles in $b$ state coupled to $J_b$ angular momentum and so on, a many-particle wave function which can be denoted as

$$\Phi^{a(N_a)\chi_a J_a, b(N_b)\chi_b J_b,\cdots}_{JMTM_T}(1,2,\ldots,A)\,, \tag{38}$$

where $\chi_i$ are the other quantum numbers. The energy levels can be also be denoted as $E^{(0)}_{JT}$.

Let us suppose that we have wave functions of $(N-1)$ identical nucleons in a single $j$-shell, which are orthonormalized, antisymmetric and characterized by certain value of $J'$ obtained by all possible ways ($\chi'$ will distinguish between different ways of coupling to the same $J'$). To get an $N$-particle wave function, totally antisymmetric and characterized by a definite value of $J$, we have to couple a single-particle wave function to an $(N-1)$-particle one and to antisymmetrize the products. The coefficients which realize this procedure are called one-particle *coefficients of fractional parentage (cfp's)* [17]:

$$\Phi^{j(N)}_{\chi JM} = \sum_{\chi' J'} \left[ j^{N-1}(\chi' J') j | \right\} j^N \chi J \left] \Phi^{j(N-1)}_{\chi' J' M'} \phi_{jm} \,, \tag{39}$$

where summation is done over all possible values of $J'$ compatible with $\vec{J} = \vec{J'} + \vec{j}$, and all values of $\chi'$ distinguishing different realizations of $(J')$. The procedure can be generalized to include the isospin quantum number $T$ as in the example above of a two-nucleon case (summation will be performed then over all possible values of $(J', T')$).

A many-particle wave functions with nucleons occupying different $j$-orbitals can be obtained first by creating antisymmetrized wave functions for groups of nucleons in each $j$-shell and then by coupling and antisymmetrization between different groups (see [42]).

## 4.3 Diagonalization of the shell-model Hamiltonian

We would like now to solve the Schrödinger equation for $\hat{H} = \hat{H}^{(0)} + \hat{V}$. Let us suppose that we have constructed a basis of many-body states, for example, by coupling single-particle states to good $(J,T)$ values using cfp's, which are eigenfunctions of the Schrödinger equation for an independent particle Hamiltonian $H^{(0)}$:

$$\hat{H}^{(0)} \Phi_{JT,k}(1,2,\ldots,A) = E^{(0)}_{JT,k} \Phi_{JT,k}(1,2,\ldots,A) \,. \tag{40}$$

The energy of a given state $(JT)k$ is a sum of single-particle energies

$$E^{(0)}_{JT,k} = \sum_{i=1}^{A} \varepsilon_i \,. \tag{41}$$

Below we will suppress the indices $(J,T)$ and denote the basis states as $|\Phi_k\rangle$, $k = 1,\ldots,d$ and corresponding energies as $E^{(0)}_k$, $k = 1,\ldots,d$ (here $d$ denotes the number of basis states $|\Phi_k\rangle$ considered, or the dimension of the model space). Then we have to take into account $\hat{V}$, i.e. we solve the eigenvalue problem

$$\hat{H}|\Psi_p\rangle = E_p|\Psi_p\rangle \,. \tag{42}$$

We are looking for the wave functions $|\Psi\rangle$ of the system in the form

$$|\Psi_p\rangle = \sum_{k=1}^{d} a_{kp} |\Phi_k\rangle \,, \tag{43}$$

with the normalization condition

$$\sum_{k=1}^{d} a^2_{kp} = 1 \qquad \text{with } \; p = 1,\ldots,d \,. \tag{44}$$

Since the Hamiltonian $\hat{H}$ is invariant in the space and isospace, its eigenstates are characterized by good values of the total angular momentum $J$ and isospin $T$. In other words, the functions $\Psi_{JT,p}$ and $\Phi_{JT,k}$ have the same labels $(JT)$ which we suppressed in the equation (43) as well to simplify the notations. Substituting (43) into equation (42), we get

$$(\hat{H}^{(0)} + \hat{V}) \sum_{k=1}^{d} a_{kp} |\Phi_k\rangle = E_p \sum_{k=1}^{d} a_{kp} |\Phi_k\rangle \,. \tag{45}$$

Multiplying this equation from the left-hand side by $\langle\Phi_l|$ and making use of the orthonormality of the basis functions $\Phi_k$, we get a system of equations

$$\sum_{k=1}^{d} H_{lk} a_{kp} = E_p a_{lp} \,, \tag{46}$$

where the matrix elements of the Hamiltonian $\hat{H}$ are given by

$$H_{lk} \equiv \langle\Phi_l|\hat{H}|\Phi_k\rangle = E_k^{(0)} \delta_{lk} + V_{lk} \,, \tag{47}$$

with $E_k^{(0)}$ representing a sum of single-particle energies and

$$V_{lk} = \langle\Phi_l|\hat{V}|\Phi_k\rangle \,. \tag{48}$$

For a two-body interaction $\hat{V}$, the matrix elements (48) are expressed in terms of the matrix elements between two-nucleon states. Thus, we have to diagonalize the matrix $H_{lk}$ and to find the eigenvalues $E_p$ and the coefficients $a_{kp}$. Since the basis is orthogonal and normalized, the eigenvectors belonging to different eigenvalues are necessarily orthogonal and can be normalized such that

$$\sum_{k=1}^{d} a_{kp} a_{kp'} = \delta_{pp'} \text{ for } E_p \neq E_{p'} \,. \tag{49}$$

If $E_p = E_{p'}$, but $p \neq p'$, the corresponding eigenvectors $\Psi_p$ and $\Psi_{p'}$ can be made orthonormal by some orthogonalization procedure.

There exist different numerical algorithms for matrix diagonalization: the Jacobi method for small matrices ($d \leq 50$), the Householder method for matrices with $50 \leq d \leq 200$, the Lanczos method for dimensions $d \geq 200$ and for giant matrices [18].

We can estimate the dimension of the configuration space in $m$-scheme for $N_\pi$ protons in the space of dimension $\Omega_\pi = \sum_{j_\pi}(2j_\pi + 1)$ and $N_\nu$ neutrons in the space of dimension $\Omega_\nu = \sum_{j_\nu}(2j_\nu + 1)$. It is given by the product of binomial coefficients

$$\left( \begin{array}{c} \Omega_\pi \\ N_\pi \end{array} \right) \left( \begin{array}{c} \Omega_\nu \\ N_\nu \end{array} \right) \tag{50}$$

This is the total dimension of the space. We can reduce it taking into account invariance of the Hamiltonian with respect to the total angular momentum $J$ and isospin $T$.

It is clear that the model space becomes quickly huge for numerical treatment as the number of nucleons increases. Only the light nuclei can be described by the *no-core calculations* [45], when all nucleons are taken into account in a space of a few or even many oscillator shells. For heavier nuclei, in practice, one usually takes into account all possible configurations of $N_\pi$ valence protons

and $N_\nu$ valence neutrons in a *valence space* (orbitals which can be occupied) beyond the *closed shell core* which is supposed to be inert. The orbitals lying energetically higher than the valence space are kept always free, however, part of low-lying excitations of valence particle to those free orbitals, as well as core excitations, should be effectively incorporated in the residual interaction (section 5).

Even though, the dimension of the space grows very quickly. For example, consider $^{60}_{30}\mathrm{Zn}_{30}$ which can be modeled by 10 valence protons and 10 valence neutrons beyond $^{40}_{20}\mathrm{Ca}_{20}$ closed-shell core in $(1p0f)$ shell-model space. The dimension of the basis states is given by

$$d(^{60}\mathrm{Zn}) = \left( \begin{array}{c} 20 \\ 10 \end{array} \right) \left( \begin{array}{c} 20 \\ 10 \end{array} \right) \approx 3.4 \times 10^{10}. \tag{51}$$

Such cases requires state-of-the-art calculations and highly efficient codes. The top list includes *m*-scheme codes ANTOINE [19], OXBASH [13], MSHELL [44], Oslo code [1], REDSTICK code [51] (for no-core shell model), while among $J(T)$-coupled codes we will mention NATHAN [19], Drexel code DUPSM [69]. Modern achievements in nuclear physics community in treating giant matrices and accuracy reached by now in the description of nuclear spectra can be found in reviews [54, 18]

As a practical example, let us calculate the energies of $0^+$ states in $^{18}$O. We will model it by two neutrons beyond $^{16}$O core in $(1s0d)$ shell-model space. First, we need to get single-particle energies. These can be extracted as difference in binding energies between $^{17}$O and $^{16}$O. The ground state of $^{17}$O is supposed to correspond to $0d_{5/2}$ configuration, while the first two excited states $1/2^+$ and $3/2^+$ can be assumed to contain dominant $1s_{1/2}$ and $0d_{3/2}$ single-particle states, respectively. Thus, we have

$$\begin{array}{l} \varepsilon_{0d_{5/2}} = BE(^{17}\mathrm{O}) - BE(^{16}\mathrm{O}) = (-131.762 + 127.619)\ \mathrm{MeV} = -4.143\ \mathrm{MeV} \\ \varepsilon_{1s_{1/2}} = \varepsilon_{0d_{5/2}} + E(^{17}\mathrm{O}(1/2^+_1)) = -3.273\ \mathrm{MeV} \\ \varepsilon_{0d_{3/2}} = \varepsilon_{0d_{5/2}} + E(^{17}\mathrm{O}(3/2^+_1)) = -0.942\ \mathrm{MeV} \end{array} \tag{52}$$

As the interaction between two valence neutrons (48), we have to know the set of two-body matrix elements (TBME's) $\langle ab;JT|V|cd;JT\rangle$ with $(JT) = (01)$. We will take the values of the two-body matrix elements from USD interaction [16] which will be described in the next section (although USD uses slightly different single-particle energies). The only necessary matrix elements are three diagonal ones

$$\begin{array}{l} \langle (0d_{5/2})^2;01|V|(0d_{5/2})^2;01\rangle = -2.82\ \mathrm{MeV} \\ \langle (0d_{5/2})^2;01|V|(0d_{3/2})^2;01\rangle = -3.186\ \mathrm{MeV} \\ \langle (1s_{1/2})^2;01|V|(1s_{1/2})^2;01\rangle = -2.125\ \mathrm{MeV} \end{array} \tag{53}$$

and three off-diagonal ones :

$$\begin{array}{l} \langle (1s_{1/2})^2;01|V|(0d_{5/2})^2;01\rangle = -0.1325\ \mathrm{MeV} \\ \langle (0d_{3/2})^2;01|V|(0d_{3/2})^2;01\rangle = -2.185\ \mathrm{MeV} \\ \langle (1s_{1/2})^2;01|V|(0d_{3/2})^2;01\rangle = -1.084\ \mathrm{MeV} \end{array} \tag{54}$$

Diagonalization of this $(3\times 3)$ matrix gives rise to three eigenvalues $E(0^+_1) = -12.95$ MeV, $E(0^+_2) = -8.10$ MeV, $E(0^+_3) = -2.79$ MeV, which leads to the following excitation spectrum with the respect to the lowset eigenstate: $E(0^+_{g.s.}) = 0$ MeV,$E(0^+_2) = 4.85$ MeV, $E(0^+_3) = 10.16$ MeV.

Exercise. Calculate excitation energies of $3^+$ states in $^{18}$O in *sd*-shell model space, if

$$\langle 1s_{1/2}0d_{5/2};31|V|1s_{1/2}0d_{5/2};31\rangle = 0.7626 \text{ MeV}$$
$$\langle 0d_{5/2}0d_{3/2};31|V|0d_{5/2}0d_{3/2};31\rangle = 0.5894 \text{ MeV}$$
$$\langle 1s_{1/2}0d_{5/2};31|V|0d_{5/2}0d_{3/2};31\rangle = 0.6741 \text{ MeV}$$

# 5 Effective interaction

The only ingredient which we have not discussed yet is the residual interaction $\hat{V}$.

## 5.1 Basic properties of the NN interaction

The bare NN interaction is the interaction between two free nucleons. It is considered in detail in the lecture of E.Epelbaum, with the special emphasize on the modern approach based on the chiral perturbation theory.

In the following sections, discussing shell evolution, we will be referring to a general structure of the NN potential, taking some of its components as a schematic effective interaction. This is why in this section we will discuss the general properties of the NN potential.

We assume that (i) nucleons are basically non-relativistic particles and they do not have any substructure, (ii) they interact via a potential, (iii) only two-body effects are considered. From the symmetry properties (see lecture of E.Epelbaum), we may construct the following components of the NN potential.

- The *central force* does not depend on the velocity (a *local* force) and contains only scalar products of $\vec{\sigma}$ and $\vec{\tau}$ operators:

$$V_C(1,2) = V_0(r) + V_\sigma(r)\vec{\sigma}_1\cdot\vec{\sigma}_2 + V_\tau(r)\vec{\tau}_1\cdot\vec{\tau}_2 + V_{\sigma\tau}(r)\vec{\sigma}_1\cdot\vec{\sigma}_2\,\vec{\tau}_1\cdot\vec{\tau}_2\,. \tag{55}$$

  The central force can be expressed alternatively using spin and isospin exchange operators:

$$\hat{P}^\sigma = \frac{1}{2}(1+\vec{\sigma}_1\cdot\vec{\sigma}_2)\,, \quad \hat{P}^\tau = \frac{1}{2}(1+\vec{\tau}_1\cdot\vec{\tau}_2)\,. \tag{56}$$

  The operator $\hat{P}^\sigma$ thus produces no change in the wave function when acting on a spin-triplet state ($S=1$) and gives a minus sign when acting on a spin-singlet state ($S=0$). Similar relations hold for $\hat{P}^\tau$. The exchange operator for spatial coordinates, $\hat{P}^r$ can be defined via the relation:

$$\hat{P}^r\hat{P}^\sigma\hat{P}^\tau = -1 \tag{57}$$

  since the two-nucleon wave function is totally antisymmetric under the interchange of all coordinates of particles 1 and 2.

  Using (56), we can rewrite (55) as

$$V_C(1,2) = V_W(r) + V_M(r)\hat{P}^r + V_B(r)\hat{P}^\sigma + V_H(r)\hat{P}^r\hat{P}^\sigma \tag{58}$$

  where

$$\begin{aligned} V_W &= V_0 - V_\sigma - V_\tau + V_{\sigma\tau} && \text{Wigner force} \\ V_M &= -4V_{\sigma\tau} && \text{Majorana force} \\ V_B &= 2V_\sigma - 2V_{\sigma\tau} && \text{Bartlett force} \\ V_H &= -2V_\tau + 2V_{\sigma\tau} && \text{Heisenberg force} \end{aligned} \tag{59}$$

Another useful way to express the central force is by using projection operators:

$$\begin{array}{ll} \hat{\Pi}_s^\sigma = \frac{1}{2}\left(1-\hat{P}^\sigma\right), & \hat{\Pi}_t^\sigma = \frac{1}{2}\left(1+\hat{P}^\sigma\right), \\ \hat{\Pi}_s^\tau = \frac{1}{2}\left(1-\hat{P}^\tau\right), & \hat{\Pi}_t^\tau = \frac{1}{2}\left(1+\hat{P}^\tau\right), \end{array} \tag{60}$$

which project onto spin or isospin single (s) or triplet (t) states. The central force can be thus expressed as

$$V_C(1,2) = V_{SE}(r)\hat{\Pi}_s^\sigma\hat{\Pi}_t^\tau + V_{TO}(r)\hat{\Pi}_t^\sigma\hat{\Pi}_t^\tau + V_{SO}(r)\hat{\Pi}_s^\sigma\hat{\Pi}_s^\tau + V_{TE}(r)\hat{\Pi}_t^\sigma\hat{\Pi}_s^\tau \tag{61}$$

where different terms mean sinlet-even (SE), triplet-odd (TO), singlet-odd (SO) and triplet-even (TE) components.

Exercise. Express strengths $V_{SE}$, $V_{TO}$, $V_{TE}$, $V_{SO}$ from (61) in terms of $V_0$, $V_\sigma$, $V_\tau$, $V_{\sigma\tau}$.

- The two-body *tensor force* also has a local character:

$$V_{TN}(1,2) = V_{TN}(r)\left(v_{t0} + v_{tt}\vec{\tau}_1\cdot\vec{\tau}_2\right)\left(\frac{(\vec{\sigma}_1\cdot\vec{r})(\vec{\sigma}_2\cdot\vec{r})}{r^2} - \frac{1}{3}\vec{\sigma}_1\cdot\vec{\sigma}_2\right). \tag{62}$$

Recoupling $\vec{\sigma}_2$ and $\vec{r}$ operators, one can get an equivalent expression:

$$V_{TN}(1,2) = V_{TN}(r)\left(v_{t0} + v_{tt}\vec{\tau}_1\cdot\vec{\tau}_2\right)\left[\vec{r}\times\vec{r}\right]^{(2)}\cdot\left[\vec{\sigma}_1\times\vec{\sigma}_2\right]^{(2)}. \tag{63}$$

Exercise. Get expression (63) from (62).

The tensor force connects only states with $S=1$, therefore it has non-zero matrix elements only between triplet states. Using projection operators (60), the tensor force can be represented as a sum of two components, tensor-even (TNE) and tensor-odd (TNO):

$$V_{TN}(1,2) = \left(V_{TNE}(r)\hat{\Pi}_s^\tau + V_{TNO}(r)\hat{\Pi}_t^\tau\right)\left[\vec{r}\times\vec{r}\right]^{(2)}\cdot\left[\vec{\sigma}_1\times\vec{\sigma}_2\right]^{(2)}. \tag{64}$$

- *Two-body spin-orbit force* has a non-local structure (velocity dependent force):

$$V_{LS}(1,2) = V_{LS}(r)\left(v_{ls0} + v_{lst}\vec{\tau}_1\cdot\vec{\tau}_2\right)\,\vec{l}\cdot\vec{S}, \tag{65}$$

where $l$ is a relative orbital angular momentum operator of a two-body state. Similarly, the two-body spin-orbit force can be expressed in terms of the projection operators as

$$V_{LS}(1,2) = V_{LSE}(r)\,\vec{l}\cdot\vec{S}\hat{\Pi}_s^\tau + V_{LSO}(r)\,\vec{l}\cdot\vec{S}\hat{\Pi}_t^\tau, \tag{66}$$

where again we see that the spin-orbit force connects only triplet states ($S=1$).

We will not consider here a second-order spin-orbit term.

The radial dependence of different terms can be parametrized using simple central potentials. On of the most useful is the Yukawa potential form,

$$V(1,2) = V_0\frac{\exp(-\mu r)}{\mu r}. \tag{67}$$

Meson-exchange theories provide a theoretical basis to the Yukawa-type radial dependence and lead naturally to a central, tensor and spin-orbit terms, with the strengths related to meson and nucleon coupling constants. The $\mu$ parameter in (67) is related to the Compton wavelength of an exchanged meson, $1/\mu = \hbar/mc$ where $m$ is the meson mass. Such potentials are characterized by an infinite core at short distances, which is not suitable for application in many-body calculations. In addition, nucleons inside a nucleus obey the Pauli principle. In the next section we will consider different ways to construct effective interaction from the bare NN force. We will also describe schematic and empirical interactions used within the shell model. In general, the central, tensor and spin-orbit components of the NN interaction with reasonably evaluated strengths can also be used within the shell model for specific purposes, as an estimate of a given force component in the in-medium interaction. We will refer to such a use in the last section.

## 5.2 Schematic interaction

Schematic interactions are parametrized functions of nucleon coordinates. They are used to calculate all TBME's in a given model space:

$$\langle ab;JT|V(1,2)|cd;JT\rangle \tag{68}$$

where $a = (n_a l_a j_a)$ denote quantum numbers of one nucleon state.

For example, an interaction between two nucleons can be imagined to be of zero-range ($\delta$-type):

$$V(1,2) = V_0\delta(\vec{r}_1 - \vec{r}_2)(1 + \alpha\vec{\sigma}_1 \cdot \vec{\sigma}_2)\,. \tag{69}$$

A few parameters, characterizing a schematic interaction, such as $V_0$ and $\alpha$ in (69), are adjusted to reproduce low-energy spectra of a few neighboring nuclei of interest. These parameters are then supposed to change from one region of the nuclear chart to another.

Another important interaction is the pairing interaction between alike nucleons. For a constant pairing force, it is defined as an extra attraction between coupled to $J = 0, T = 1$ pairs of nucleons, which results in only non-zero TBME's of the type

$$\langle a^2;01|V_{pairing}(1,2)|b^2;01\rangle = -(-1)^{l_a+l_b}\frac{1}{2}G\sqrt{(2j_a+1)(2j_b+1)}\,, \tag{70}$$

where $G$ is the strength, and zero matrix elements otherwise.

The last schematic interaction we would like to mention here is the quadrupole-quadrupole interaction which is necessary, in particular, its proton-neutron part, to describe rotation of deformed nuclei. This is a $\lambda = 2$ component of the general (proton-neutron) multipole-multipole interaction (a separable interaction) of the type:

$$V(1,2) = \sum_\lambda \chi_\lambda (Q_\lambda \cdot Q_\lambda) = \sum_\lambda \chi_\lambda\, r_\pi^\lambda r_\nu^\lambda Y_\lambda(\Omega_\pi)\cdot Y_\lambda(\Omega_\nu)\,. \tag{71}$$

## 5.3 Empirical interaction

Schematic interactions possess only local predictive power. A pragmatic approach to get a residual interaction is to consider all TBME's in a given model space as free parameters. The energy eigenvalues obtained after diagonalization can be represented as linear combinations of these parameters. Hence, the TBME's of the residual interaction can be adjusted to reproduce experimental low-energy spectra of nuclei from the model space by a least-square fit procedure.

The approach allows to get a good description of nuclei in a given model space. The drawback is that as the model space increases, the number of parameters increases drastically (15 TBME's for $(0p)$-shell, 63 TBME's in $(1s0d)$-shell model space, 195 TBME's in $(1p0f)$ shell model space and so on). To reach convergence, one uses the so-called linear combination method [16, 54]. Its meaning is to choose the most important linear combinations of TBME's to be determined in a fit. The interaction found in this way describes very accurately the data. The examples of empirical interactions are the $(0p)$-shell interaction of Cohen and Kurath [21], the so-called universal $(1s0d)$-interaction (USD) [16, 14], the $(1p0f)$-shell GXPF1 interaction [34, 35].

## 5.4 Microscopic interaction

The most fundamental way to get the two-nucleon interaction to be exploited in the many-body calculations is to derive it from a bare NN potential for free nucleons in a vacuum, by taking into account medium effects, the Pauli principle and truncated model space. This is why such an interaction is called an *effective interaction*. We will briefly describe below two different renormalization procedures[1] which help to eliminate the short-range attractive part of the NN interaction and thus can serve as a first step to the construction of the microscopic effective interaction.

### 5.4.1 Many-body perturbation theory and $G$-matrix

The traditional way to get the effective shell-model interaction was via calculation of the so-called $G$-matrix and then computation of the effective interaction between two nucleons in the valence space. We will only sketch the basic ideas behind the approach based on the time-independent perturbation theory (see Refs. [10, 40, 33] for detail), while the time-dependent perturbation theory formalism can be find elsewhere [40, 33].

We have to solve the Schrödinger equation

$$\hat{H}\Psi = (\hat{H}^{(0)} + \hat{V})\Psi = E\Psi\,, \tag{72}$$

where $\hat{H}^{(0)}$ is an unperturbed $A$-nucleon Hamiltonian as defined by (4), $\Psi$ is the true wave function, which should be expanded in basis of the solutions for $\hat{H}^{(0)}$ as

$$\Psi = \sum_{k=1}^{\infty} a_k \Phi_k\,. \tag{73}$$

However, we cannot solve this equation in a full Hilbert space and we replace this expansion by a similar one, but in a restricted model space:

$$\Psi^M = \sum_{k\in M} a_k \Phi_k\,. \tag{74}$$

Thus, we would like to solve the Schrödinger equation for a model wave function, however, to get true eigenvalues. This means that we need to change also the interaction $V$ by an effective one $V_{eff}$:

$$\hat{H}_{eff}\Psi^M = (\hat{H}^{(0)} + \hat{V}_{eff})\Psi^M = E\Psi^M \tag{75}$$

[1] Other techniques are developed for no-core shell model [45] or coupled-cluster approaches [23] which are beyond the scope of the present course.

To continue we introduce projection operators $\hat{P}$ and $\hat{Q}$ with the following properties which project the true wave function onto and off the model space $M$:

$$\begin{aligned} \hat{P} &= \sum_{k\in M} |\Phi_k\rangle\langle\Phi_k| \\ \hat{Q} &= \sum_{k\notin M} |\Phi_k\rangle\langle\Phi_k| \end{aligned} \tag{76}$$

These operators satisfy the following decoupling properties:

$$\begin{aligned} &\hat{P}+\hat{Q}=1\,, \\ &\hat{P}^2=\hat{P}, \quad \hat{Q}^2=\hat{Q}\,, \\ &\hat{P}\hat{Q}=\hat{Q}\hat{P}=0\,, \end{aligned} \tag{77}$$

and they commute with the unperturbed Hamiltonian:

$$\left[\hat{P},\hat{H}^{(0)}\right]=\left[\hat{Q},\hat{H}^{(0)}\right]=0\,. \tag{78}$$

Starting from two equations

$$\begin{aligned} \hat{P}(\hat{H}-E)\Psi=0 \\ \hat{Q}(\hat{H}-E)\Psi=0 \end{aligned} \tag{79}$$

one can get the following relation between $V_{eff}$ and $V$:

$$\hat{V}_{eff}=\hat{V}+\hat{V}\frac{\hat{Q}}{E-\hat{H}^{(0)}}\hat{V}_{eff} \tag{80}$$

and a similar relation between the truncated wave function $\Psi^M$ and a true one $\Psi$:

$$\Psi=\Psi^M+\frac{\hat{Q}}{E-\hat{H}^{(0)}}\hat{V}\Psi\,. \tag{81}$$

`Exercise: Obtain eqs. (80) and (81).`

The inconvenience of these equations is that $V_{eff}$ and $\Psi^M$ depend on the true energy $E$ which is not known. However, representing $E$ as

$$E=E_c^{(0)}+\Delta E_c+E_v^{(0)}+\Delta E_{cv}\,, \tag{82}$$

where $E_c^{(0)}$ is an unperturbed core energy, $E_c^{(0)}+\Delta E_c$ is the true core energy, $E_v^{(0)}$ is an unperturbed valence energy and $\Delta E_{cv}$ is the rest, one can show [10] that eq. (80) can be rewritten for valence nucleons as

$$\begin{aligned} \hat{V}_{eff} &= \hat{V}+\hat{V}\frac{\hat{Q}}{E_v-\hat{H}_v^{(0)}}\hat{V}_{eff} \\ &= \hat{V}+\hat{V}\frac{\hat{Q}}{E_v-\hat{H}_v^{(0)}}\hat{V}+\hat{V}\frac{\hat{Q}}{E_v-\hat{H}_v^{(0)}}\hat{V}\frac{\hat{Q}}{E_v-\hat{H}_v^{(0)}}\hat{V}+\ldots\,, \end{aligned} \tag{83}$$

where $\hat{H}_v^{(0)}$ is an unperturbed Hamiltonian for valence particles. These series can be evaluated by using a diagrammatic technique. The summations include only the special class of diagrams, *linked and folded diagrams* [10].

The standard approach to this equation was to sum first an infinite class of diagrams, called *ladder diagrams* which result in the Brückner's reaction $G$-matrix, solution of the Bethe-Goldstone equation [8]:

$$\hat{G}(\omega) = \hat{V} + \hat{V}\frac{\hat{Q}_{2p}}{\omega - \hat{H}_{2p}^{(0)}}\hat{G}(\omega)\,, \tag{84}$$

where $H_{2p}^{(0)}$ is an unperturbed Hamiltonian of the intermediate two-particle, the Pauli operator $\hat{Q}_{2p}$ produces a non-vanishing result only if it acts on a pair of particles, both of which are beyond the Fermi level. The parameter $\omega$ represents the so-called starting energy at which $G$-matrix is evaluated. It is considered as a softer interaction compared to the bare NN potential. Evaluation of the $G$-matrix for finite nuclei can be found in Refs. [5, 33].

As a second step, the $G$-matrix is used to calculate the effective interaction for the model space to be used in the shell-model calculations:

$$\begin{aligned}\hat{V}_{eff} &= \hat{G} + \hat{G}\frac{\hat{Q}'}{E_v - \hat{H}_v^{(0)}}\hat{V}_{eff} \\ &= \hat{G} + \hat{G}\frac{\hat{Q}'}{E_v - \hat{H}_v^{(0)}}\hat{G} + \hat{G}\frac{\hat{Q}'}{E_v - \hat{H}_v^{(0)}}\hat{G}\frac{\hat{Q}'}{E_v - \hat{H}_v^{(0)}}\hat{G} + \ldots .\end{aligned} \tag{85}$$

where the prime on the projection operator $\hat{Q}'$ indicates that the ladder diagrams are excluded. Thus the effective interaction is given as a perturbation expansion in orders of $G$. The leading order term in this expression is given by the $G$-matrix itself. Calculations for finite nuclei in valence spaces show necessity to go beyond, taking into account higher order terms, such as core-polarization and so on [41]. More details and the current status can be found in Refs. [33].

In spite of much progress in development of techniques to get $V_{eff}$ via (85), numerical evaluation of the last equation is very complicated. In addition, it is not clear whether the series converges, i.e. whether a next order term in the expansion is smaller than the previous one. It is very difficult to go beyond the second order term in perturbation and it is hard to incorporate three-nucleon interactions.

### 5.4.2 $V_{low-k}$

Recently, a new approach to get a soft interaction has been developed. The high-momentum component of the bare $NN$-interaction is integrated out down to a given cut-off momentum $\Lambda$ within the renormalization group approach, resulting in a so-called $V_{low-k}$ (see [9] and the lecture of Th. Duguet in this volume). For a cut-off $\Lambda \sim 2.1$ fm$^{-1}$, low-momentum interactions derived from different bare NN potentials are very similar to each other. The soft interaction brings promising results in studies of nuclear matter properties. It is possible to incorporate three-body forces provided by effective-field theory potentials [70, 26, 27] (and lecture of E. Epelbaum in this volume), what is very important for application in nuclear spectroscopy within the shell-model approach.

To be applied in the shell model calculations for heavy nuclei in a valence space, core-polarization and other diagrams should be added to $V_{low-k}$. For first applications within the shell model see [22] and references therein.

Up to now, either microscopic interaction based on the $G$-matrix, or on $V_{low-k}$, derived from two-nucleon potential, leads to a reasonable description of nuclei with two or a few valence nucleons beyond a closed shell core in a one-oscillator shell valence space. As soon as the model space

increases, the agreement deteriorates. The plausible reason is the absence of many-body forces, in particular, the lack of a three-body force. As shows a systematic analysis, it is always mainly the *monopole part* of the interaction which requires modifications [59]. This is why for successful description, microscopically obtained TBME's are subjected to an adjustment to known experimental data in the model space. This can be performed either by minimal monopole changes [59, 43, 48], or by a least-square fit [34, 54]. As the number of TBME's gets important, a microscopic effective interaction serves as a starting point to get a good realistic interaction. The descriptive and predictive power of such interactions is very high (see [18] for numerous examples).

# 6 Multipole-multipole decomposition

To proceed with the analysis of the changes in the shell structure and appearance or disappearance of magic numbers we will need to deal with the multipole-multipole decomposition of the shell-model Hamiltonian which has to be performed in the occupation number formalism, or sometimes called second quantization.

## 6.1 Second-quantization

In a second quantization formalism, we introduce nucleon creation operator $a^\dagger_\alpha$ which creates a single-particle state $|\alpha\rangle$ acting on a vacuum state $|0\rangle$:

$$|\alpha\rangle = a^\dagger_\alpha |0\rangle \tag{86}$$

and the corresponding annihilation operator

$$\langle\alpha| = \langle 0| a_\alpha \,, \tag{87}$$

with the annihilation operator $a_\alpha$ being a Hermitean conjugate of the creation operator $a^\dagger_\alpha$:

$$a_\alpha = \left(a^\dagger_\alpha\right)^\dagger \tag{88}$$

The coordinate representation of the single-particle state $\alpha$ is given by the single-particle wave function discussed above:

$$\langle\vec{r}|\alpha\rangle = \phi_\alpha(\vec{r}) \tag{89}$$

These fermion creation and annihilation operators satisfy (anti)commutation relations:

$$\begin{aligned} \left\{a^\dagger_\alpha, a_\beta\right\} = a^\dagger_\alpha a_\beta + a_\beta a^\dagger_\alpha = \delta_{\alpha\beta} \,, \\ \left\{a^\dagger_\alpha, a^\dagger_\beta\right\} = \left\{a_\alpha, a_\beta\right\} = 0 \,. \end{aligned} \tag{90}$$

Thus an $A$-nucleon antisymmetric state can be expressed as

$$|\alpha_1\alpha_2\ldots\alpha_A\rangle = a^\dagger_{\alpha_A} a^\dagger_{\alpha_{A-1}} \ldots a^\dagger_{\alpha_2} a^\dagger_{\alpha_1} |0\rangle \,. \tag{91}$$

Operators have also to be expressed in a second-quantization formalism. A symmetric one-body operator acting on a system of $A$ identical fermions,

$$\hat{O} = \sum_{k=1}^{A} \hat{O}(\vec{r}_k) \,, \tag{92}$$

is characterized by its matrix elements between one-body states:

$$\langle\alpha|\hat{O}|\beta\rangle = \int \phi^*_\alpha(\vec{r})\hat{O}(\vec{r})\phi_\beta(\vec{r})d\vec{r}. \tag{93}$$

It is easy to verify that the second-quantized expression for this operator is given by

$$\hat{O} = \sum_{\alpha\beta}\langle\alpha|\hat{O}|\beta\rangle a^\dagger_\alpha a_\beta\,. \tag{94}$$

For example, the number operator reads as

$$\hat{N} = \sum_{\alpha\beta}\langle\alpha|\hat{1}|\beta\rangle a^\dagger_\alpha a_\beta = \sum_\alpha a^\dagger_\alpha a_\alpha\,. \tag{95}$$

Similarly, a symmetric two-body operator acting on a system of $A$ identical fermions

$$\hat{T} = \sum_{j<k=1}^{A}\hat{T}(\vec{r}_k,\vec{r}_j) \tag{96}$$

is characterized by its matrix elements between normalized antisymmetric two-body states:

$$\langle\alpha\beta|\hat{T}|\gamma\delta\rangle = \int \phi^*_\alpha(\vec{r}_1)\phi^*_\beta(\vec{r}_2)\hat{T}(\vec{r}_1,\vec{r}_2)\left(1-\hat{P}_{12}\right)\phi_\gamma(\vec{r}_1)\phi_\delta(\vec{r}_2)d\vec{r}_1 d\vec{r}_2\,, \tag{97}$$

where $\hat{P}_{12}$ is an exchange operator. It can be shown that this operator may be equivalently expressed in a second-quantization formalism as

$$\hat{T} = \frac{1}{4}\sum_{\alpha\beta\gamma\delta}\langle\alpha\beta|\hat{T}|\gamma\delta\rangle a^\dagger_\alpha a^\dagger_\beta a_\delta a_\gamma. \tag{98}$$

The shell model Hamiltonian (3), containing a one-body term ($\hat{H}^{(0)}$), and a two-body term ($\hat{V}$), can be thus rewritten in a second-quantization formalism in the following way:

$$\hat{H} = \sum_\alpha \varepsilon_\alpha a^\dagger_\alpha a_\alpha + \frac{1}{4}\sum_{\alpha\beta\gamma\delta}\langle\alpha\beta|\hat{V}|\gamma\delta\rangle a^\dagger_\alpha a^\dagger_\beta a_\delta a_\gamma, \tag{99}$$

where the one-body term is diagonal in the harmonic-oscillator basis.

## 6.2 Second-quantization and angular momentum coupling

In the nuclear shell model the angular momentum is conserved, therefore, it is convenient to work with angular momentum coupled states. Creation operators $a^\dagger_\alpha$ represent spherical tensors of rank $j_\alpha$. As in section 4.2, instead of a single-partile state notation $\alpha$, we will use notation $a = (n_a l_a j_a)$ to denote three quantum labels and a separate notation for the angular momentum projection $m_a$. A creation operator $a^\dagger_\alpha$ will be represented as $a^\dagger_{am_a}$. A state of two fermions coupled to a certain angular momentum $J$ can be constructed using the Clebsch-Gordan coefficients:

$$\begin{aligned} |ab;JM\rangle &\equiv |(n_a l_a j_a)(n_b l_b j_b);JM\rangle = -\frac{1}{\sqrt{1+\delta_{ab}}}\sum_{m_a m_b}(j_a m_a j_b m_b|JM)a^\dagger_{am_a}a^\dagger_{bm_b}|0\rangle \\ &= -\frac{1}{\sqrt{1+\delta_{ab}}}\left[a^\dagger_a \times a^\dagger_b\right]^J_M|0\rangle\,. \end{aligned} \tag{100}$$

Here $\delta_{ab} \equiv \delta_{n_a n_b}\delta_{l_a l_b}\delta_{j_a j_b}$. Similarly, in using the isospin formalism, one may need to express an antisymmetric two-body state characterized by good $J$ and $T$ values:

$$|ab;JMTM_T\rangle = -\frac{1}{\sqrt{1+\delta_{ab}}}\left[a^\dagger_{a\frac{1}{2}} \times a^\dagger_{b\frac{1}{2}}\right]^{JT}_{MM_T}|0\rangle\,. \tag{101}$$

For further discussion, we will need to transform the residual interaction (a two-body term from (99)) to a coupled form using angular momentum coupling:

$$\hat{V} = -\frac{1}{4}\sum_{abcd,J}\langle ab;JM|\hat{V}|cd;JM\rangle\sqrt{2J+1}\sqrt{(1+\delta_{ab})(1+\delta_{cd})}\left[\left[a^\dagger_a \times a^\dagger_b\right]^{(J)} \times [\tilde{a}_c \times \tilde{a}_d]^{(J)}\right]^{(0)}_0\,. \tag{102}$$

Here we introduced annihilation operators with the phase $\tilde{a}_{cm_c} = (-1)^{j_c+m_c}a_{c,-m_c}$ which have good transformation properties under rotations. Expression (102) can be generalized to the case of isospin formalism as

$$\hat{V} = -\tfrac{1}{4}\sum_{abcd,JT}\sqrt{(2J+1)(2T+1)}\sqrt{(1+\delta_{ab})(1+\delta_{cd})}\langle ab;JMTM_T|\hat{V}|cd;JMTM_T\rangle \left[\left[a^\dagger_{a\frac{1}{2}} \times a^\dagger_{b\frac{1}{2}}\right]^{(JT)} \times \left[\tilde{a}_{c\frac{1}{2}} \times \tilde{a}_{d\frac{1}{2}}\right]^{(JT)}\right]^{(0)}_0\,. \tag{103}$$

The form of the residual interaction as in (102)-(103) is called a *particle-particle* representation. For further consideration, we will need also another form, called a *particle-hole* (or multipole) representation. To get it, we have to interchange the operators $a^\dagger_b$ and $\tilde{a}_c$, using commutation relations and preserving a coupled form of the expression. Assuming that the model space contains only orbitals from one or two neighboring oscillator shells (otherwise extra terms would appear in the expression below due to the presence of the orbitals with the same $(lj)$ quantum numbers, but different $n$-values), we obtain a multipole representation the two-body interaction (102):

$$\hat{V} = \frac{1}{4}\sum_{abcd,\lambda} w^\lambda_{abcd}\sqrt{2\lambda+1}\sqrt{(1+\delta_{ab})(1+\delta_{cd})}\left[\left[a^\dagger_a \times \tilde{a}_c\right]^{(\lambda)} \times \left[a^\dagger_b \times \tilde{a}_d\right]^{(\lambda)}\right]^{(0)}_0\,. \tag{104}$$

The parameters $w^\lambda_{abcd}$ can be obtained from the two-body matrix elements of the residual interaction $\hat{V}$ entering expression (102). For a proton-neutron part of $\hat{V}$, we have

$$w^\lambda_{abcd} = \sum_J (2J+1)(-1)^{j_c+j_b-\lambda-J}\left\{\begin{array}{ccc} j_a & j_b & J \\ j_d & j_c & \lambda \end{array}\right\}\langle ab;JM|\hat{V}|cd;JM\rangle\,. \tag{105}$$

Eq. (104) can be generalized to the isospin quantum number:

$$\hat{V} = \frac{1}{4}\sum_{abcd,\lambda\tau} w^{\lambda\tau}_{abcd}\sqrt{(2\lambda+1)(2\tau+1)}\sqrt{(1+\delta_{ab})(1+\delta_{cd})}\left[\left[a^\dagger_{a\frac{1}{2}} \times \tilde{a}_{c\frac{1}{2}}\right]^{(\lambda\tau)} \times \left[a^\dagger_{b\frac{1}{2}} \times \tilde{a}_{d\frac{1}{2}}\right]^{(\lambda\tau)}\right]^{(0)}_0\,. \tag{106}$$

The multipole expansion of the residual interaction (104) or (106) is extremely important. It allows to separate the shell-model Hamiltonian into the *monopole part* [3, 59, 75, 18], i.e. all one-body and $\lambda = 0$ terms in (104) or $(\lambda\tau) = (00)$ and $(01)$ terms in the expression (106), and the rest called a *multipole part*. In the next two sections we will discuss their physical meaning and their role in the formation of nuclear spectra.

## 6.3 Monopole Hamiltonian and effective single-particle energies

In the proton-neutron formalism, if the model space contains only one or two neighboring oscillator shells, the monopole Hamiltonian has a diagonal form and can be expressed in terms of neutron and proton number operators:

$$\hat{H}_{mon} = \sum_a \varepsilon_a^\nu \hat{N}_a^\nu + \sum_a \varepsilon_a^\pi \hat{N}_a^\pi + \sum_{ab} \bar{V}_{ab}^{\nu\pi} \hat{N}_a^\nu \hat{N}_b^\pi + \sum_{a\le b} \frac{\hat{N}_a^\nu(\hat{N}_b^\nu - \delta_{ab})}{1+\delta_{ab}} \bar{V}_{ab}^{\nu\nu} + \sum_{a\le b} \frac{\hat{N}_a^\pi(\hat{N}_b^\pi - \delta_{ab})}{1+\delta_{ab}} \bar{V}_{ab}^{\pi\pi} . \quad (107)$$

The matrix elements with a bar represent angular-momentum averaged TBME's, or *centroids* of the interaction:

$$\bar{V}_{ab}^{\rho\rho'} = \frac{\sum_J \langle ab;JM|V|ab;JM\rangle (2J+1)}{\sum_J (2J+1)} \quad (108)$$

where $\rho, \rho'$ stand for $\pi$ or $\nu$ (a proton or a neutron), $a, b$ run over valence orbitals and angular momentum $J$ takes all allowed values.

`Exercise. Show that the centroid of a separable multipole-multipole proton-neutron interaction (71) is non-zero only for its monopole (`$\lambda = 0$`) component.`

The monopole Hamiltonian (107) represents a *spherical mean field* as extracted from the interacting shell model. The single-particle states in this average potential are called *effective single-particle energies (ESPE's)*. These can be defined as a nucleon separation energy for an unoccupied orbital or the extra energy necessary to extract a nucleon from a fully occupied orbital (taken with an opposite sign).

From expression (107) one can get that in a series of isotopes or isotones, ESPE of a given $a$-state of $\rho$-type of nucleons can be calculated as

$$\tilde{\varepsilon}_a^\rho(A) = \varepsilon_a^\rho(A_0) + \sum_b \bar{V}_{ab}^{\rho\rho'} \langle \hat{N}_b^{\rho'} \rangle \quad (109)$$

where $\rho'$ denote neutrons or protons, respectively.

A given configuration (or particle distribution over valence orbitals) is characterized by certain nucleon occupation numbers $(N_a, N_b, \ldots)$ in the valence space of the oscillator orbitals $a$, $b$, etc. In the case of normal filling (all orbitals are occupied up to a Fermi level), $N_a$, $N_b$, etc are integer numbers and the eigenenergy of the monopole Hamiltonian can be simply calculated for a given two-body interaction using (107). For example, the ESPE of the $\nu 0f_{7/2}$ orbital at $Z=8$, $N=20$ is the difference between the total energy obtained from (107) for $^{28}$O in its ground state and $^{29}$O with an extra neutron in the $0f_{7/2}$ state. It is important to note that nuclei with one particle or one hole beyond the closed shell core are the best examples to check the monopole field, since in these cases other particle-particle correlations are often negligible and one can associate single-particle centroids with the eigenstates of the monopole Hamiltonian. In Fig. 2 we show calculated neutron ESPE's for $N=20$ isotones in the $(1s0d1p0f)$ shell-model space, evaluated only for nuclei with fully occupied sub-shells: $^{28}$O, $^{34}$Si, $^{36}$S and $^{40}$Ca. It is well seen that ESPE's are not constant as a function of proton number, but represent linear functions according to the following equation:

$$\tilde{\varepsilon}_a^\nu(A) = \varepsilon_a^\nu(^{28}\mathrm{O}) + \sum_b \bar{V}_{ab}^{\nu\pi} N_b^\pi , \quad (110)$$

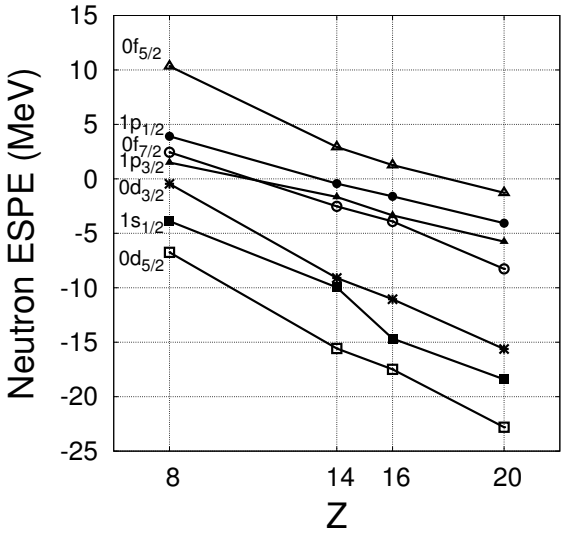


Figure 2: Variation of the neutron ESPE's in $N = 20$ isotones from O to Ca calculated using the realistic interaction [50].

where summation is performed over proton orbitals. Thus, the shift of the ESPE's is due to the monopole part of the proton-neutron matrix elements (108). The bigger the overlap of the proton and neutron radial wave functions and the higher the $j$-values of the orbitals considered will lead, in general, to more drastic changes.

We see very well the shell structure. For nuclei from $A = 34$ to $A = 40$, we notice two separate oscillator shells, the $(1s0d)$ shell and the higher-lying $(1p0f)$ shell with an energy gap of about 7 MeV between them. This is in line with our knowledge on the shell structure for stable nuclei. However, below $^{34}$Si, we may notice that the neutron $0d_{3/2}$ state comes closer to the neutron $(1p0f)$ shell, creating a big gap between the $1s_{1/2}$ and $0d_{3/2}$ states. This is a phenomenon which will be discussed in the next section.

In nuclei with partially filled orbitals other particle-particle correlations become important and the role of the monopoles is not easily seen. One particular case of nuclei can however be easily incorporated in (109). These are nuclei adjacent to semimagic ones, i.e. having an extra proton (neutron) beyond a closed shell and an even number of nucleons of the other kind. Then the most important particle-particle correlations at low energies are the pairing correlations among identical nucleons and these can be taken into account within the BCS approximation (see [28, 65, 30, 63] for details). For example, let us consider odd-A Cu-isotopes ($Z = 29$) which can be modeled by a valence proton and an even number of valence neutrons in the $(1p0f_{5/2}0g_{9/2})$ shell-model space beyond the $^{56}$Ni closed-shell core. We are interested in the shift of the proton ESPE's starting from $^{57}$Cu and to heavier Cu-isotopes as a function of neutron number. Expression (109) can be directly applied with the exception that we need a more precise determination of the neutron occupation numbers than normal filling. We know that the pairing correlations are important in semi-magic nuclei. Calculating neutron occupation probabilities $v^2_{j_b}$ from the BCS equations for

valence neutrons, assuming a pure pairing force with a strength $G = 23/A$, we get

$$\tilde{\varepsilon}^{\pi}_{a}(A) = \varepsilon^{\pi}_{a}(^{57}\mathrm{Cu}) + \sum_{b} \bar{V}^{\pi\nu}_{ab}(2j_b+1)v^2_{j_b} \tag{111}$$

where label $a$ refers to the proton orbitals and $b$ runs over neutron orbitals. Proton ESPE's from (111) calculated from a realistic interaction are shown in Fig. 3(b).

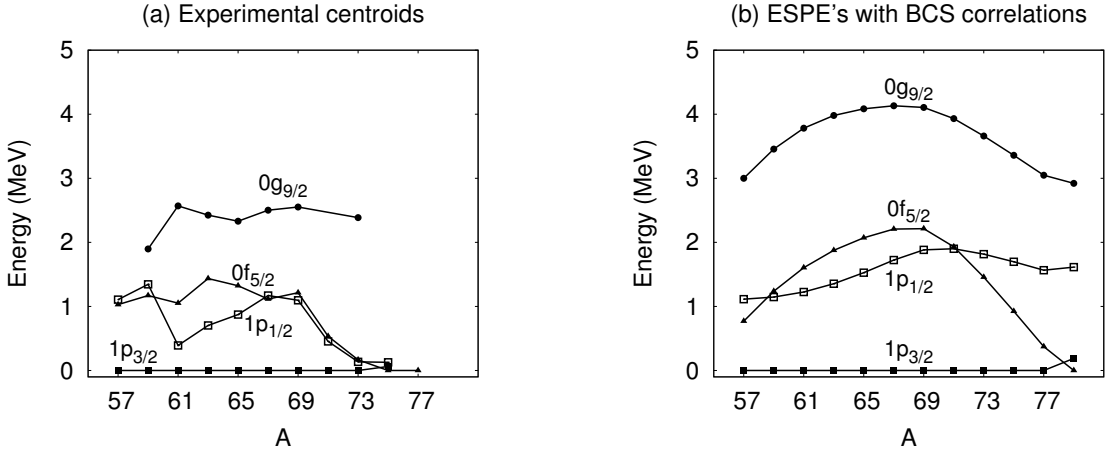


Figure 3: (a) Experimental centroids (if information available) of single-particle states in odd-A Cu-isotopes; (b) Proton ESPE's in odd-A Cu-isotopes from the realistic interaction [48], including the BCS correlations among valence neutrons according to eq. (111).

The monopole part is tightly connected with the single-particle energies defined from spectroscopic strengths and may be extracted from experimental data. Following Ref. [4, 68], let us consider one-nucleon transfer reactions.

- In the case of a closed-shell nucleus, if a nucleon is transferred to an orbital from a valence space in a stripping reaction, an ESPE of this orbital is defined via

$$\tilde{\varepsilon}_{nlj} = \sum_{f} S^{+j}_{fi} \mathcal{E}^{+j}_{fi}\,, \tag{112}$$

  where $\mathcal{E}^{+j}_{fi} = E_{n+1,k_fJ_f} - E_{nk_iJ_i}$ is an excitation energy of the final state of one-nucleon transfer reaction. Here we take into account that final state may carry different $J_f$ values and the $S$-coefficient is related to a spectroscopic factor,

$$S^{+j}_{fi} = \frac{\left|\langle n+1, k_fJ_f||a^{+}_{nlj}||nk_iJ_i\rangle\right|^2}{(2j+1)(2J_i+1)}\,. \tag{113}$$

- In the case of a closed-shell nucleus, if a nucleon is removed from an occupied orbital from a valence space in a pick-up reaction, an ESPE of this orbital (a one-hole state) can be expressed as

$$\tilde{\varepsilon}_{nlj} = \sum_f S_{fi}^{-j} \mathcal{E}_{fi}^{-j} , \tag{114}$$

where $\mathcal{E}_{fi}^{-j} = E_{nk_iJ_i} - E_{n-1,k_fJ_f}$ is an excitation energy of the final state of one-nucleon transfer reaction and

$$S_{fi}^{-j} = \frac{\left| \langle n, k_i J_i || a_{nlj}^{+} || n-1, k_f J_f \rangle \right|^2}{(2j+1)(2J_i+1)} . \tag{115}$$

- In the case of a nucleus with valence particles (an open-shell nucleus), to get an ESPE of a partially filled orbital, we have to consider both possibilities, to populate this state by a nucleon and to remove one nucleon from this state, i.e.

$$\tilde{\varepsilon}_{nlj} = \sum_f S_{fi}^{+j} \mathcal{E}_{fi}^{+j} + \sum_f S_{fi}^{-j} \mathcal{E}_{fi}^{-j} , \tag{116}$$

where $S_{fi}^{\pm j}$ are defined above and satisfy the following sum rule:

$$\sum_f S_{fi}^{+j} + \sum_f S_{fi}^{-j} = 1 . \tag{117}$$

It can be shown [68] that such defined single-particle energies can be obtained in the shell-model formalism as one-nucleon separation energies from the monopole Hamiltonian (107).

Experimental determination of the single-particle energies, however, is rather difficult in nuclei with open shells since it requires measurements of the full spectroscopic strength. Even near closed shells only part of the strength is known. This complicates the comparison between theory and experiment. As an example, in Fig. 3(a) we show experimental centroids in Cu-isotopes obtained from stripping reactions on Ni-isotopes from (112). In spite of the fact that the lowest $3/2^+$ states and $1/2^+$ states contain more than half of the proton single-particle contribution of $1p_{3/2}$ and $1p_{1/2}$ states, respectively, much more data on $5/2^-$ and $9/2^+$ states in Cu-nuclei is desired. Beyond $^{65}$Cu, all indicated states are only lowest levels of a given spin and parity (β-decay experiments for heavy Cu's). The effective interaction used in the theoretical calculation [63] does not allow to reproduce correctly the change of the ground state spin and parity to $5/2^-$ observed already in $^{75}$Cu and expected in heavier odd-A isotopes, however, it reproduces the rapid lowering of the $0f_{5/2}$ state as the occupation of the neutrons $0g_{9/2}$ orbital increases (from $^{69}$Cu to $^{79}$Cu).

## 6.4 Multipole Hamiltonian

The multipole part of the shell-model Hamiltonian can be defined as the total Hamiltonian minus its monopole part, i.e.

$$H_{mult} = H - H_{mon} = \sum_{abcd,\lambda\neq 0} w_{abcd}^{\lambda} \left[ \left[ a_a^{\dagger} \times \tilde{a}_c \right]^{(\lambda)} \times \left[ a_b^{\dagger} \times \tilde{a}_d \right]^{(\lambda)} \right]_0^{(0)} . \tag{118}$$

It contains basically all multipoles of the two-body interaction, except for $\lambda = 0$ terms. The most important terms represent isoscalar and isovector pairing, quadrupole-quadrupole interaction, hexadecapole-hexadecapole term, spin-flip term and other. For the full extraction and discussion we will refer to Ref. [24, 18].

# 7 Shape coexistence and "islands of inversion"

There are numerous indications that the shell structure changes with changing $N/Z$ ratio. Characteristic shell gaps responsible for extra stability at certain values of $N$ and/or $Z$ (magic numbers) are not the same in nuclei near the valley of stability and in very neutron-rich or neutron-deficient nuclei. How to understand and describe quenching of a certain shell gap and the onset of deformation? The mechanism, discussed below, leads to a phenomenon called *shape coexistence* (appearance of spherical and deformed structures at similar excitation energies), well known in heavier nuclei, and it can lead even to deformed ground states in lighter nuclei with large neutron excess characterized by "magic" values of $N$ or $Z$ (nuclei belonging to the so-called *"islands of inversion"*).

## 7.1 Shape coexistence near closed shells

Shape coexistence in nuclei around closed shells is known for long time already [29, 72]. As an example we will consider here Pb-isotopes. $^{208}_{82}\mathrm{Pb}_{126}$ is a well-known doubly-magic nucleus, its ground state is spherical and first excited states lie very high in energy. Fig. 4 shows some selected low-lying states of even-even Pb-isotopes from $^{206}$Pb down to the very light $^{184}$Pb as neutrons empty the $(0h_{9/2}1f2p0i_{13/2})$ shell-model space. We note an excited $0^+$ state which appears rather high in energy in $^{206}$Pb and quickly lowers as more and more neutrons are removed . The minimum is reached near $^{186}$Pb where about half of the neutron shell is filled. These $0^+$ states are known to correspond to an oblate quadrupole-deformed nuclear shape [72, 37]. Some other members of the bands are known around $^{198}$Pb (in Fig. 4 the oblate-deformed states are shown by lines of green color in online edition).

Within the shell model they can be approximated as two-particle-two-hole ($2p$-$2h$) excitations across the magic $Z = 82$ shell gap (see schematic picture on the right side of the Fig. 5), called *intruder configurations*. Their energy can be evaluated following the approach developed in Ref. [30]:

$$E_{intruder} = 2\left(\varepsilon(j_\pi) - \varepsilon(j'_\pi)\right) - \Delta E^{\pi\pi}_{pair} + \Delta E^{\pi\nu}_{M} + \Delta E^{\pi\nu}_{Q} \,, \tag{119}$$

where $\varepsilon(j_\pi)$ and $\varepsilon(j'_\pi)$ denote proton single-particle energies in the two major shells ($j_\pi$ is the orbital in the upper shell to which the particles are promoted and $j'_\pi$ is the orbital in the formerly filled shell from where two particles are excited). In the independent single-particle model, such a $2p$-$2h$ excitation energy would be as high as $2(\varepsilon(j_\pi) - \varepsilon(j'_\pi)) \simeq 7$ MeV. However, two-body correlations compensate for such an increase (see left side of Fig. 5 for energy contributions from different terms of (119) provided $j_\pi$ runs over proton $0h_{9/2}$ and $0i_{13/2}$ orbitals, while $j'_\pi$ stands for the proton $2s_{1/2}$ orbital). There is a gain in pairing energy $\Delta E^{\pi\pi}_{pair}$ due to the creation of a particle pair at $j_\pi$ and a hole pair at $j'_\pi$ (with respect to a closed-shell configuration). Then, there is a monopole correction $\Delta E^{\pi\nu}_{M}$ to the single-particle energy due to the changing total proton-neutron interaction as neutrons are removed (109). Finally, open shell configurations manifest quadrupole-quadrupole interaction $\Delta E^{\pi\nu}_{Q}$, which being estimated in a bosonic approximation [30] shows a parabolic trend as a function of valence neutrons (Fig. 5). The total energy of the $2p$-$2h$ intruder thus shows a spectacular descent from $^{208}$Pb to $^{186}$Pb leading to rather good agreement with the experimental trend.

In general, multi-particle-multi-hole ($np$-$nh$) excitations across a magic shell gap can take place in nuclei near shell closures. In the case of Pb-nuclei, many prolate quadrupole-deformed bands

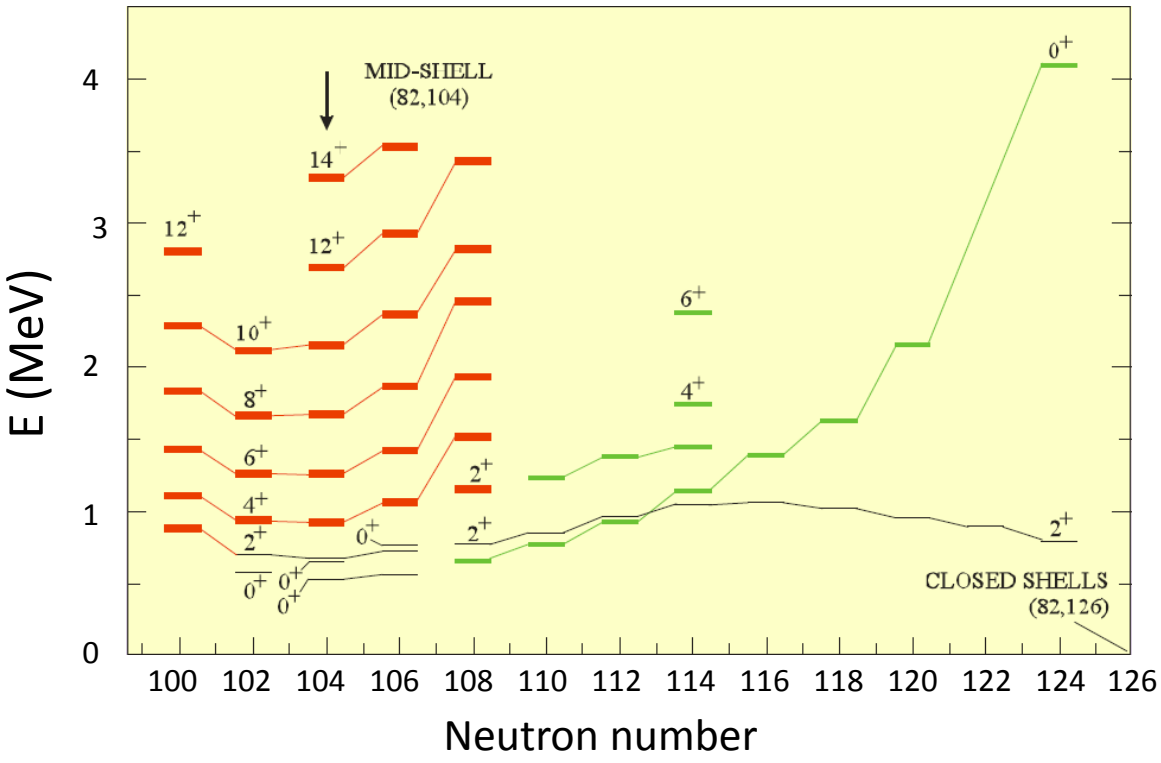


Figure 4: Low-energy states in Pb-isotopes (from K. Heyde).

have been recently observed in $^{182-190}$Pb which are shown by thick lines (of red color in online edition) in Fig. 4. These are states based on $4p$-$4h$ proton excitations across the $Z = 82$ shell gap. In particular, three coexisting $0^+$ states — spherical, oblate and prolate deformed — have been identified below 1 MeV (three lowest states) in $^{186}$Pb [2].

The pairing interaction and the quadrupole-quadrupole interaction are contained in the multipole part of the shell-model Hamiltonian. So, generally speaking, the relative energy between spherical and deformed configurations is determined by a competition of the monopole term and the other multipole terms of the nuclear Hamiltonian.

## 7.2 "Islands of inversion"

In light neutron-rich nuclei this phenomenon becomes even more pronounced, when deformed configurations may not only be observed at very low energies, coexisting with the spherical ground state shape, but even become ground state configurations themselves. In addition, spin and parity of the ground states of odd-$A$ neighbors confirm inversion of single-particle level structure inherent to stable nuclei. After $^{11}$Be with an unexpected $1/2^+$ ground state, the first discovery attracting overall attention was the determination of the $3/2^+$ ground state of $^{31}$Na [67], signifying that this $N = 20$ nucleus is deformed at low energies. Later on, it was found out that $^{32}$Mg$_{20}$ is deformed in its ground state from the low-lying first excited $2^+$ state and a large $B(E2; 2^+_1 \rightarrow 0^+_{g.s.})$ value. Since then numerous experimental and theoretical investigations of the nuclear structure have been

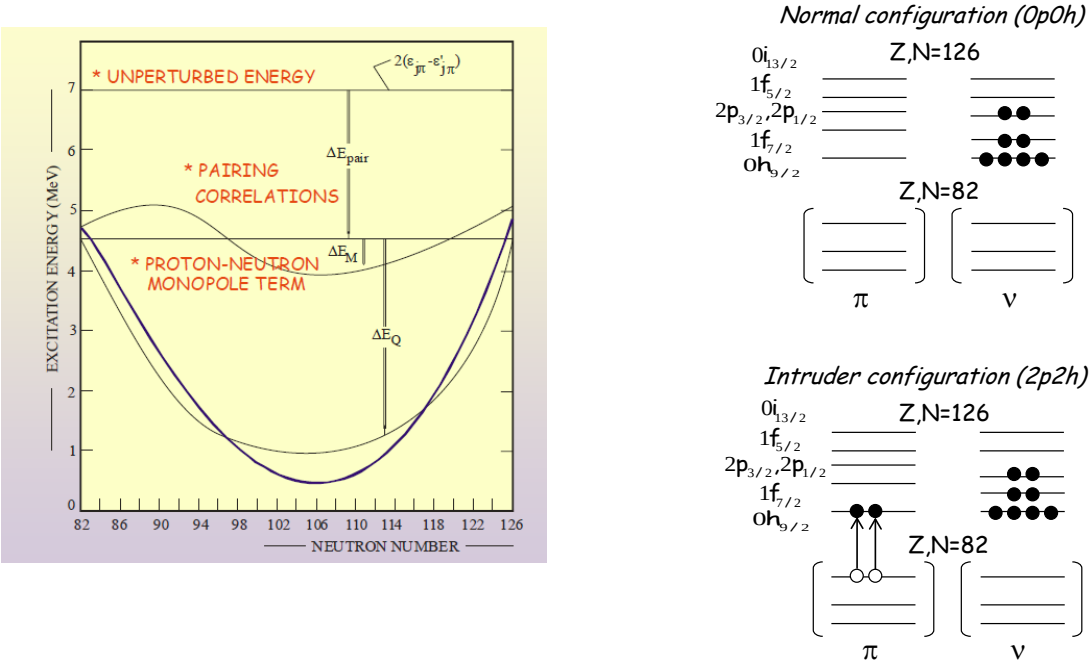


Figure 5: Schematic evaluation of the intruder energy in neutron-deficient Pb-isotopes (from [30]).

Table 2: Experimental data on Mg-isotopes around $N = 20$.

| Nucleus | $^{30}$Mg$_{18}$ | $^{32}$Mg$_{20}$ | $^{34}$Mg$_{22}$ |
|---|---|---|---|
| $E(2_1^+)$ (MeV) | 1.48 | 0.89 | 0.67 |
| $E(4_1^+)$ (MeV) | | (2.3) | (2.13) |
| $B(E2;2_1^+ \to 0_{g.s.}^+)$ (e$^2$.fm$^4$) | 59(5) | 90(16) | 126(25) |

performed in nuclei far from stability. Breaking of the ground state sphericity is now known at magic numbers $N = 20$ in F, Ne, Na and Mg nuclei, at $N = 28$ in neutron-rich S, Si, Mg, at $N = 40$ in Cr-nuclei and around. On the other hand, appearance of new magic numbers such as $N = 16$ for O-isotopes has been reported as well. For an overview of the experimental situation in various mass regions see Ref. [66] and the lecture of O. Sorlin in this volume.

In the shell model, deformed states in $N = 20$ nuclei are associated with $np$-$nh$ excitations of neutrons across $N = 20$ shell gap. Table 2 shows some experimental data on three Mg-isotopes with $N = 18, 20, 22$. Indeed, it is well seen that $^{32,34}$Mg are characterized by low-lying $2^+$ states and large $B(E2)$ values inherent to deformed rotors. Table 3 (from Ref. [18]) presents calculated properties of $^{32}$Mg for the normal configuration ($0p$-$0h$ — all nucleons are confined in $(1s0d)$ shell) and intruder configurations ($2p$-$2h$ — two neutrons are fixed in the $(1p0f)$ shells and therefore two holes are created in the $(1s0d)$ shell-model space), see also Fig. 6. It is evident that spectroscopic data are much better reproduced for an intruder configuration in $^{32}$Mg, rather than for a normal spherical configuration. Appearance of such $np$-$nh$ excitations low in energy is explained again by the energy balance between two parts of the shell-model Hamiltonian — a

Table 3: Theoretical calculation [18] for $^{32}$Mg assuming normal or intruder configurations.

| Configurations in $^{32}$Mg | Normal ($0p$-$0h$) | Intruder ($2p$-$2h$) |
|---|---|---|
| $E(0^+_{g.s.})$ (MeV) | 0 | 0 (-1.1) |
| $E(2^+_1)$ (MeV) | 1.69 | 0.93 |
| $E(4^+_1)$ (MeV) | 2.93 | 2.33 |
| $B(E2;2^+_1 \rightarrow 0^+_{g.s.})$ ($e^2.fm^4$) | 36 | 98 |

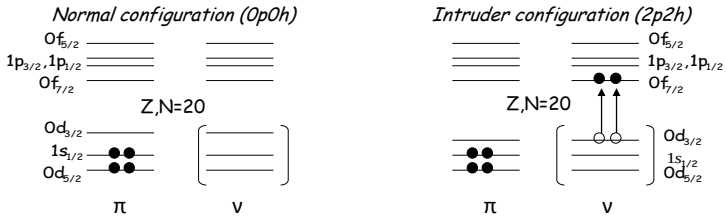


Figure 6: Normal and intruder configurations in $^{32}$Mg.

monopole term and higher multipole terms. The neutron ESPE's obtained from a recently developed realistic interaction [50] are shown in Fig. 2 and have already been discussed. A schematic approach to estimate the intruder energy as was done for Pb-nuclei in (119) has been worked out in Ref. [31]. The monopole energy gap between $\nu 0d_{3/2}$ and $\nu 0f_{7/2}$ is strongly reducing in isotones below $^{34}$Si (see Fig. 2). In addition, due to the gain in pairing energy while creating a pair of neutron particles in $(1p0f)$ shell and a pair of neutron holes in $(1s0d)$ shell and due to the increase in quadrupole-quadrupole interaction energy in an open-shell configuration, such a $2p$-$2h$ intruder becomes favorable in $^{32}$Mg. Fig. 7 shows the numerical result obtained from the diagonalization

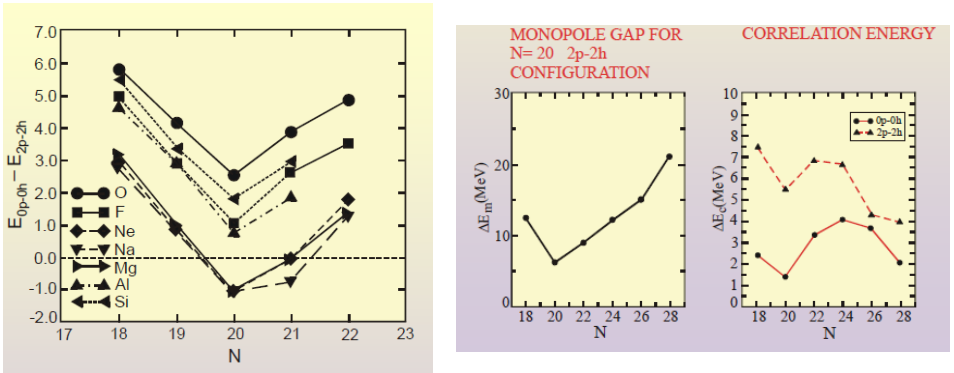


Figure 7: Figures taken from Ref. [20]: energy difference between normal $0p-0h$ and intruder $2p-2h$ configurations in neutron-rich nuclei around $N = 20$ (left plot); monopole energy gap and correlation energy in Mg-isotopes around $N = 20$ (two right plots).

of the nuclear Hamiltonian. On the left side there is an energy difference between $0p$-$0h$ and $2p$-$2h$ configurations, predicting deformed ground states for $N = 20, 21$ Mg-Na-Ne nuclei. On the right side, there are two plots showing the monopole energy gap in Mg-isotopes and the correlation energy from the multipole Hamiltonian. We see that the decrease of the $N = 20$ spherical shell gap and the increase in correlation energy (mainly of a quadrupole-quadrupole type) in open-shell configurations energetically favors deformed ground states in $N = 20, 21$ Mg-Na-Ne nuclei and, thus, evidence the disapperance of the $N = 20$ shell closure in this region.

A huge correlation energy can be created in multi-particle-multi-hole excitations ($4p$-$4h$ or $8p$-$8h$) in closed-shell nuclei, leading to excited superdeformed bands in doubly-magic nuclei and nearby, such as $^{16}$O, $^{40}$Ca, $^{36}$Ar, etc (see Ref. [18] for details).

So, large spherical shell gaps obtained from a monopole Hamiltonian is a necessary condition to have certain magic numbers. At the same time, the multipole part of the Hamiltonian is responsible for the correlation energy (an energy gain from particle-particle correlations, such as pairing, quadrupole-quadrupole correlations, etc). The interplay between these two terms of the shell-model Hamiltonian determines the structure of the ground state. The contribution from the multipole interaction (or the magnitude of the correlation energy) depends on the number of valence particles and the orbitals they occupy. It is important, therefore, to study the mechanism behind changes in the spherical shell structure from stable nuclei to nuclei with large neutron excess. This is the topic of the next section, where only the monopole Hamiltonian is discussed.

# 8 Shell evolution and nuclear forces

## 8.1 Spin-isospin exchange central term versus tensor force

The question what particular component of the nuclear interaction is responsible for the appearance or disappearance of magic numbers was first raised in 2001 [53]. The authors studied the behavior of neutron ESPE's in $N = 16$ isotones. The structure of $^{32}S_{16}$ at low energies is well described in the shell model as a nucleus with 8 valence protons and 8 valence neutron in the $(1s0d)$ shell-model space beyond an $^{16}$O 'inert' core (see Fig. 8). At the same time, $^{24}O_{16}$ is characterized by the large shell gap between neutron $0d_{3/2}$ and $1s_{1/2}$ single-particle states. The former $(1s0d)$ shell is splitted and a new $N = 16$ magic number appears. In the extreme single-particle picture with normal filling of orbitals, $^{32}S_{16}$ differs from $^{24}O_{16}$ by 6 protons which completely occupy the $0d_{5/2}$ orbital. While protons fill the $0d_{5/2}$ orbital, the neutron $0d_{3/2}$ state comes much lower in energy, i.e. there is an extra well manifested attraction between a proton in the $0d_{5/2}$ state and a neutron in the $0d_{3/2}$ state, i.e. the centroid $\bar{V}^{\pi\nu}_{0d_{5/2}0d_{3/2}}$ is large and negative. This particular feature is characteristic for a spin-isospin-exchange component of the *NN* interaction (the last term in (55)). So, the conclusion of the authors of Ref. [53] was that the spin-isospin-exchange term governs the shell structure.

However, later on studying heavier nuclei, it has been noticed [55, 64] that throughout the nuclear chart, an ESPE of a certain neutron (proton) $nl, j = l \pm 1/2$ comes lower in energy while a proton (neutron) orbit with $n'l', j' = l' \mp 1/2$ is being filled. This means that there is a particularly strong attraction between proton and neutron in the orbitals with different spin-to-orbital orientation of the angular momentum, even when these orbitals do not have the same orbital angular momenta ($l \neq l'$). This effect could not been explained by a central spin-isospin exchange term, however, it was very much in agreement with the following analytical property inherent to the

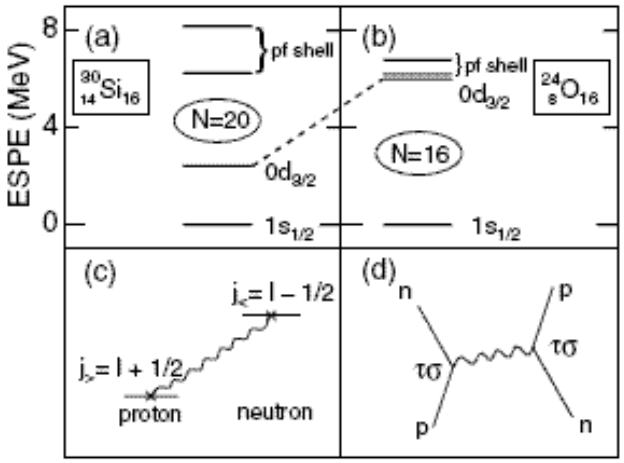


Figure 8: From Ref. [53]: schematic neutron ESPE's in $^{32}$S and $^{24}$O (a,b); attraction between the proton $j = l + 1/2$ orbital and the neutron $j = l - 1/2$ orbital (c) and the proposed spin-isospin-exchange mechanism of this attraction (d).

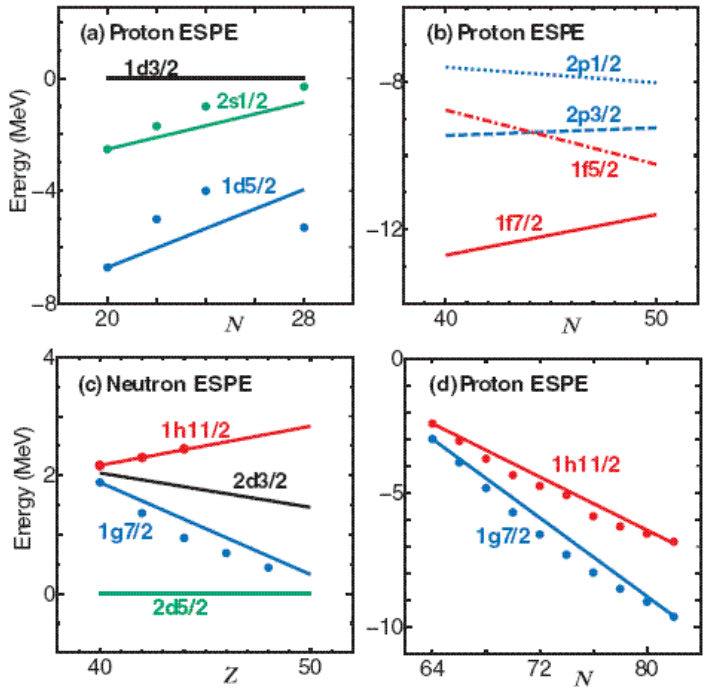


Figure 9: Figure from Ref. [55]: proton (neutron) ESPE's as a function of $N$ ($Z$) as due to the tensor force against experimental data (points). (a) Proton ESPE's in Ca-isotopes; (b) proton ESPE's in Ni-isotopes; (c) neutron ESPE's in $N = 51$ isotones; (d) proton ESPE's in Sb-isotopes (tensor + a common monopole shift).

tensor operator (62):

$$(2j_> + 1)\bar{V}^{\pi\nu}_{j_> j'} + (2j_< + 1)\bar{V}^{\pi\nu}_{j_< j'} = 0 \tag{120}$$

where $j_> = l + 1/2$ and $j_< = l - 1/2$ are proton (neutron) orbitals and $j'$ refers to a neutron (proton) orbital. This means that the centroids $\bar{V}^{\pi\nu}_{j_> j'}$ and $\bar{V}^{\pi\nu}_{j_< j'}$, calculated for a tensor interaction (62), are of opposite sign. Therefore, if we consider ESPE's of $j_>$ and $j_<$ orbitals for a tensor operator only, we get them shifting in opposite ways, while $j'$ is being filled. Amazingly, such a property may indeed be found experimentally in many cases, some of which can be seen in Fig. 9 (taken from Ref. [55]). For example, experimental energies of proton single-particle states in Ca-isotopes obtained from the information on the proton hole states from $^{39}K_{20}$ to $^{47}K_{28}$ are shown in Fig. 9(a). It is seen that while neutrons fill the $0f_{7/2}$ single-particle orbital (the normal filling is assumed), the splitting between the proton $0d_{5/2}$ and $0d_{3/2}$ orbitals is reducing.

We can notice similar trends of theoretical ESPE's obtained from realistic interactions (full interaction), which points out on the important role of the tensor component. For example, in Fig. 2 we see that while protons fill the $0d_{5/2}$ orbital (from O to Si), the splitting between neutron $0f_{7/2}$ and $0f_{5/2}$ orbitals decreases. The opposite effect is observed when protons fill the $0d_{3/2}$ orbital (from S to Ca) i.e. the corresponding splitting increases. A similar but less pronounced behavior is noticed for the neutron $1p_{3/2}$ and $1p_{1/2}$ orbitals.

The authors of Ref. [55] calculated the effect of the tensor force by estimating its strength as given by $(\pi + \rho)$-exchange potential (two mesons which are responsible in the meson-exchange picture of the nuclear force for the creation of a tensor component (62)). Since the radial part is infinitely large when approaching zero, a radial cut-off at $r = 0.7$ fm was imposed. The tensor force, estimated in such a way, could indeed account for the increase in the proton $0d_{5/2}$-$0d_{3/2}$ energy splitting between $^{40}$Ca and $^{48}$Ca, as well as it could describe the increase of the neutron $0h_{11/2}$-$0g_{7/2}$ energy splitting in $N = 51$ isotones and of the proton $0h_{11/2}$-$0g_{7/2}$ energy splitting in Sb-isotopes (Fig. 9(c,d)). The two latter cases were conjectured to be indirectly due to the effect of the tensor force [55]. It has been thus suggested [55] that it is the tensor force which mainly manifests in ESPE shifts and, therefore, governs evolution of the nuclear shell structure.

The work within the shell model has stimulated a large number of investigations using mean-field approaches (see e.g. [6] and references therein). It is worth noting that standard phenomenological interactions, such as Skyrme or Gogny force, most frequently used in mean-field calculations, do not include a tensor term [7]. Provided its importance, a tensor term should be introduced and the parameters re-adjusted, what up to now, is not satisfactorily reached yet (see, e.g. Ref. [60, 74, 6]).

In spite of the indirect evidence, the role of the tensor force still needs to be clarified. It is undoubtedly an important part of the bare NN force, however, as was discussed in section 5, the NN interaction is subjected to a strong renormalization before it can be handled as an effective interaction in many-body calculations within a restricted model space [33]. It is not straightforward to trace how the tensor component will become renormalized amongst the other terms contributing to the NN interaction. Moreover, many shell-model interactions having high descriptive and predictive power are of empirical type. Even the effective interactions, maximally preserving their microscopic origin (based on a $G$-matrix), need further phenomenological correction (see e.g., [59, 50]).

In addition, recent shell-model studies based on large-scale calculations using a realistic effective interaction in the heavy Sn-nuclei region [49] conclude on the absence of a characteristic effect expected to result from a tensor force component on the basis of the almost equivalence of

two centroids, $\bar{V}^{\pi\nu}_{0g_{9/2}0h_{11/2}}$ and $\bar{V}^{\pi\nu}_{0g_{7/2}0h_{11/2}}$.

These arguments lead to the application of yet another technique to analyze the structure of an effective shell-model interaction and pin down the role of its different components.

## 8.2 Spin-tensor decomposition

In this section we will describe a method which allows to determine the role of different components of the in-medium NN interaction in nuclear shell evolution. It is based on a *spin-tensor decomposition* of the two-particle interaction, known for many years [25, 38, 61, 39, 73, 15, 52]. In a given model space, a complete set of TBME's determines the properties of nuclei ranging within this space. Since the interacting particles are spin $1/2$ fermions (nucleons), one can construct from their spin operators a complete set of linear operators in a two-particle spin space:

$$S_1^{(0)} = 1,\ S_2^{(0)} = [\vec{\sigma}_1 \times \vec{\sigma}_2]^{(0)},\ S_3^{(1)} = \vec{\sigma}_1 + \vec{\sigma}_2\,,$$
$$S_4^{(2)} = [\vec{\sigma}_1 \times \vec{\sigma}_2]^{(2)},\ S_5^{(1)} = [\vec{\sigma}_1 \times \vec{\sigma}_2]^{(1)},\ S_6^{(1)} = \vec{\sigma}_1 - \vec{\sigma}_2\,.$$

By coupling the spin tensor operators with the corresponding rank tensors in the configuration space one can construct scalar interaction terms. The most general two-body interaction can then be written as

$$V(1,2) \equiv V = \sum_{k=0,1,2} \left( S^{(k)} \cdot Q^{(k)} \right) = \sum_{k=0,1,2} V^{(k)}. \tag{121}$$

Here, $V^{(0)}$ and $V^{(2)}$ represent the central and tensor parts of the effective *NN* interaction (see eqs. (55) and (63), respectively). The $V^{(k=1)}$ term contains the so-called symmetric ($S^{(1)}_{i=3}$) and antisymmetric ($S^{(1)}_{i=5,6}$) spin-orbit operators [39]. To obtain the matrix elements for the different multipole components in $jj$-coupling, the following procedure can be exploited. First, one has to transform the TBME's between normalized and antisymmetrized states from $jj$-coupling to *LS*-coupling in a standard way:

$$\begin{aligned}
&\langle (n_a l_a, n_b l_b) : LS, JMTM_T | V(1,2) | (n_c l_c, n_d l_c) : L'S', JMTM_T \rangle = \\
&\frac{1}{\sqrt{(1+\delta_{n_a n_b}\delta_{l_a l_b})(1+\delta_{n_c n_d}\delta_{l_c l_d})}} \sum_{j_a j_b j_c j_d} \begin{pmatrix} l_a & 1/2 & j_a \\ l_b & 1/2 & j_b \\ L & S & J \end{pmatrix} \begin{pmatrix} l_c & 1/2 & j_c \\ l_d & 1/2 & j_d \\ L' & S' & J \end{pmatrix} \times \\
&\sqrt{(1+\delta_{ab})(1+\delta_{cd})} \langle (ab) JMTM_T | V(1,2) | (cd) JMTM_T \rangle\,,
\end{aligned} \tag{122}$$

where $a = (n_a, l_a, j_a)$ and so on, and the factor in the brackets is a generalized $9j$-symbol:

$$\begin{pmatrix} l_a & 1/2 & j_a \\ l_b & 1/2 & j_b \\ L & S & J \end{pmatrix} = \sqrt{(2j_a+1)(2j_b+1)(2L+1)(2S+1)} \begin{Bmatrix} l_a & 1/2 & j_a \\ l_b & 1/2 & j_b \\ L & S & J \end{Bmatrix}. \tag{123}$$

The *LS*-coupled matrix elements of $V^{(k)}$ can be calculated from the *LS*-coupled matrix elements of $V$:

$$\begin{aligned}
&\langle (n_a l_a, n_b l_b) : LS, JMTM_T | V^{(k)} | (n_c l_c, n_d l_c) : L'S', JMTM_T \rangle = (2k+1)(-1)^J \begin{Bmatrix} L & S & J \\ S' & L' & k \end{Bmatrix} \\
&\sum_{J'} (-1)^{J'} (2J'+1) \begin{Bmatrix} L & S & J' \\ S' & L' & k \end{Bmatrix} \langle (n_a l_a, n_b l_b) : LS, J'MTM_T | V | (n_c l_c, n_d l_d) : L'S', J'MTM_T \rangle,
\end{aligned} \tag{124}$$

Finally, *LS*-coupled matrix elements of $V^{(k)}$, for each $k$, can be transformed to $jj$-coupled matrix elements and used for further investigation. Note that for a given set of quantum numbers of two-body states, the matrix elements of $V$ are a sum of the matrix elements of its three components $V^{(k)}$.

In addition, using the projection operators, one can select different components of the effective interaction that connect two-nucleon states with specific values of the total spin $S$, isospin $T$ and parity $(-1)^L$. This means that one can represent the central component $V^{(0)}$ as given by eq. (61), the spin-orbit part of the vector component $V^{(1)}$ can be expressed in the form of eq. (66) and the tensor component $V^{(2)}$ can be expressed as in eq. (64). Based on the selection rules in *LS*-coupling, we can distinguish between all these terms, i.e. separate triplet-even (TE), triplet-odd (TO), singlet-even (SE) and singlet-odd (SO) channels of the central part, as well as the even and odd channels of the symmetric spin-orbit and tensor part.

Previously, the spin-tensor decomposition was applied to study the structure of TBME's of different interactions and/or their contribution in building nuclear spectra [38, 39, 73, 15, 52, 34]. It is very advantageous to apply the decomposition to study the monopole Hamiltonian, since the contribution of the different terms to the two-body centroids is additive [68, 62].

Spin-tensor decomposition may give a quantitative answer to the question how each component of the effective interaction contributes to the energy gap evolution in a series of isotopes and isotones. The only drawback is that the decomposition described above requires that the model space contains all spin-orbit partners within a given oscillator shell. This limits the region of applicability to the lighter nuclei. However, many interesting observations can still be extracted, as will be demonstrated below.

In Table 4 we analyze shell-gap variations in $N = 20$ isotones shown in Fig. 2. ESPE's were calculated using a recently elaborated interaction in $(1s0d1p0f)$ shell-model space [50]. The total energy shift (first line) is a sum of the central, vector and tensor contributions. For example, the decrease of the splitting between neutron $0d_{3/2}$ and $1s_{1/2}$ by 2.57 MeV, going from $^{28}$O to $^{34}$Si (Table 4, column 2), turns out to result from the combined effect of the central part (1.87 MeV), in particular, in its triplet-even channel, and the tensor part of the nuclear interaction (1.06 MeV).

Similarly, the increase of the gap between the neutron $0d_{3/2}$ and $0f_{7/2}$ orbitals when going from $^{28}$O to $^{34}$Si and onwards from $^{36}$S to $^{40}$Ca (columns 3 and 4 of Table 4) is a joint effect of the central and tensor component of the effective interaction. This is an important manifestation of the tensor force in this region. Due to the fact that at $N=20$ the above two neutron orbitals have (i) the same radial quantum number, and, (ii) a different spin-to-orbital orientation, a large and negative tensor contribution of $-1.93$ MeV results for the variation of the gap between the $0d_{3/2}$ and $0f_{7/2}$ orbitals when filling the $0d_{3/2}$ orbital with protons (from $^{36}$S to $^{40}$Ca). This large tensor shift, however, is almost fully cancelled by the central contribution of 1.99 MeV. The combined effect results in only a slight overall decrease of the $N=20$ shell gap from $^{40}$Ca to $^{36}$S and $^{34}$Si, thereby preserving the semi-magic nature of the latter nuclei. At the same time, while filling the $0d_{5/2}$ orbital with protons (from $^{28}$O to $^{34}$Si), due to the change in the spin-to-orbital orientation with respect the proton $0d_{3/2}$ orbital, the tensor contribution remains large but changes its sign (1.96 MeV). This enforces the central contribution (2.17 MeV) and results in a rapid decrease of the $N=20$ shell gap below $^{34}$Si which is at the origin of the "island of inversion" around $^{32}$Mg (deformed ground state).

Fig. 10(a) shows calculated proton ESPE's in Ca-isotopes (one-hole states) using the same interaction [50]. There is a crossing of the $1s_{1/2}$ and the $0d_{3/2}$ orbitals and, in addition, a lowering

Table 4: Contribution of different spin-tensor operators to the energy splitting variations $\Delta(j,j') \equiv \varepsilon_j - \varepsilon_{j'}$ in $N=20$ isotones.

| Energy gap | $\nu(0d_{3/2},1s_{1/2})$ MeV | $\nu(0f_{7/2},0d_{3/2})$ MeV | $\nu(0f_{7/2},0d_{3/2})$ MeV |
|---|---|---|---|
| Filling orbital | $\pi 0d_{5/2}$ $^{28}$O$\rightarrow^{34}$Si | $\pi 0d_{5/2}$ $^{28}$O$\rightarrow^{34}$Si | $\pi 0d_{3/2}$ $^{36}$S$\rightarrow^{40}$Ca |
| Total | **-2.57** | **3.68** | **0.21** |
| Central | **-1.87** | **2.17** | **1.99** |
| TE | -1.58 | 2.23 | 2.48 |
| TO | -0.68 | -0.31 | -0.11 |
| SE | 0.71 | -0.45 | 0.01 |
| SO | -0.32 | 0.70 | -0.39 |
| Vector | **0.36** | **-0.45** | **0.15** |
| LS | -0.05 | -0.10 | -0.16 |
| even | -0.12 | -0.06 | 0.25 |
| odd | 0.07 | -0.04 | -0.41 |
| ALS | 0.41 | -0.35 | 0.31 |
| Tensor | **-1.06** | **1.96** | **-1.93** |
| even | -0.78 | 1.31 | -1.28 |
| odd | -0.28 | 0.66 | -0.65 |

Table 5: Contribution of different spin-tensor operators to the energy splitting variations $\Delta(j,j') \equiv \varepsilon_j - \varepsilon_{j'}$ in Ca-isotopes (columns 2-3) and in $N=28$ isotones (columns 4-5).

| Energy gap | $\pi(0d_{3/2},0d_{5/2})$ MeV | $\pi(0d_{3/2},1s_{1/2})$ MeV | $\nu(1p_{3/2},0f_{7/2})$ MeV | $\nu(1p_{3/2},0f_{7/2})$ MeV |
|---|---|---|---|---|
| Filling orbital | $\nu 0f_{7/2}$ $^{40}$Ca$\rightarrow$ $^{48}$Ca | $\nu 0f_{7/2}$ $^{40}$Ca$\rightarrow$ $^{48}$Ca | $\pi 0d_{5/2}$ $^{36}$O$\rightarrow^{42}$Si | $\pi 0d_{3/2}$ $^{44}$S$\rightarrow^{48}$Ca |
| Total | **-2.33** | **-3.16** | **1.60** | **1.81** |
| Central | **-0.21** | **-1.58** | **2.03** | **1.31** |
| TE | 0.62 | -1.19 | 2.03 | 1.02 |
| TO | -0.03 | 0.25 | -0.25 | -0.14 |
| SE | -0.50 | -0.57 | -0.02 | 0.18 |
| SO | -0.30 | -0.07 | 0.28 | 0.25 |
| Vector | **0.61** | **0.06** | **0.23** | **-0.18** |
| LS | 0.09 | -0.15 | 0.11 | 0.15 |
| even | 0.60 | 0.25 | 0.22 | -0.27 |
| odd | -0.51 | -0.40 | -0.11 | 0.41 |
| ALS | 0.52 | 0.21 | 0.12 | -0.33 |
| Tensor | **-2.73** | **-1.64** | **-0.67** | **0.68** |
| even | -1.59 | -0.96 | -0.43 | 0.43 |
| odd | -1.14 | -0.68 | -0.24 | 0.26 |

of the energy gap between the $0d_{3/2}$ and the $0d_{5/2}$ orbitals when going from $^{40}$Ca to $^{48}$Ca. This is well confirmed experimentally. In Table 5 we present a detailed analysis of the role of different components in the evolution of the gaps. It is seen (columns 2) that the lowering of the gap between proton $0d_{5/2}$ and $0d_{3/2}$ orbitals as neutrons fill the $0f_{7/2}$ orbital is mainly due to the tensor force. However, it is the central part, combined with the contribution from the tensor force, which reduces the gap between proton $0d_{3/2}$ and $1s_{1/2}$ orbitals when approaching $^{48}$Ca (column 3). Finally, let us consider the evolution of the $N = 28$ shell gap, i.e. the reduction of the neutron

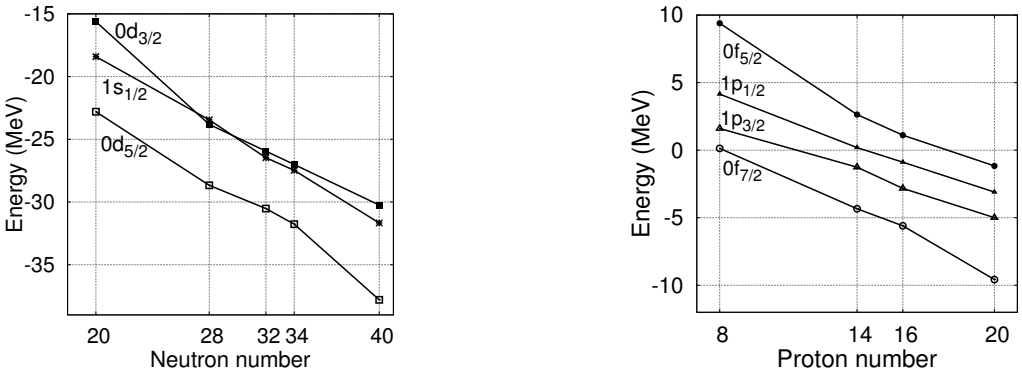


Figure 10: (a) Variation of ESPE's for proton-hole states in Ca-isotopes; (b) variation of neutron ESPE's in $N=28$ isotones using the realistic interaction [50].

$1p_{3/2}$–$0f_{7/2}$ energy difference from $^{48}$Ca to lighter isotopes (see Fig. 10(b)). To start with, these two orbitals have different radial quantum numbers. Therefore, the radial overlap contributing to the $\bar{V}^{\pi\nu}_{0d_{3/2}0f_{7/2}}$ centroid is larger than the radial overlap contributing to the $\bar{V}^{\pi\nu}_{0d_{3/2}1p_{3/2}}$ centroid. As can be seen from Table 5 (columns 4–5), the contributions from the central and tensor terms are dominating. Since both the $0f_{7/2}$ and $1p_{3/2}$ orbital are 'spin-up' oriented ($j_> = l+1/2$), the tensor term contributes in a similar way to the energy shift when protons fill the $0d_{3/2}$ orbital ($\bar{V}^{(k=2)\pi\nu}_{0d_{3/2}0f_{7/2}}$ and $\bar{V}^{(k=2)\pi\nu}_{0d_{3/2}1p_{3/2}}$ are both positive). The same happens when protons fill the $0d_{5/2}$ orbital ($\bar{V}^{(k=2)\pi\nu}_{0d_{5/2}0f_{7/2}}$ and $\bar{V}^{(k=2)\pi\nu}_{0d_{5/2}1p_{3/2}}$ are both negative). The overall difference in sign is due to the different relative spin to orbital orientation of the neutron orbitals (both $(j_>{}^{\nu} = l^{\nu} + 1/2)$ relative to the proton orbitals ($j^{\pi} = l^{\pi} \pm 1/2$)). Due to the difference in absolute value of the centroids, in particular, due to different radial overlaps for $\nu 0f$-$\pi 0d$ versus $\nu 1p$ -$\pi 0d$, the positive and negative tensor contributions to the energy centroid do not cancel. They result in a shift of 0.68 MeV and $-0.67$ MeV while filling the $0d_{3/2}$ or $0d_{5/2}$ orbital, respectively. Adding this tensor energy shift to the central plus vector energy shift results in a reduction of the $N=28$ shell gap going from $^{48}$Ca to $^{44}$S and from $^{42}$Si to $^{36}$O. This situation contrasts the $N=20$ shell gap evolution discussed above.

These examples illustrate that in the discussion of shell gap evolution, it is mandatory to take into account what particular orbitals are considered. Both the central and tensor term represent important ingredients, together with the magnitude of the radial overlaps involved.

# 9 Conclusion

The nuclear shell model is applied to discuss the changes in the shell structure of nuclei ranging from stable to very neutron-rich species. In particular, the special attention is payed to the competition between magicity, inherent to closed-shell configurations, and deformation, developing in open-shell configurations. The spherical single-particle energies and the shell gaps are defined by the monopole part of the shell-model Hamiltonian, while the particle-particle correlations are contained in the higher-multipole part. The interplay between these two terms determines the relative energy of different configurations and, thus, helps to understand such phenomena as shape coexistence in semi-magic nuclei and around and the appearance of "islands of inversion" in very-neutron rich nuclei.

Variations of single-particle energies and the related shell gaps have been explored in a long chain of isotopes or isotones in a few regions of nuclear chart. The question of whether a particular force of an effective NN interaction drives changes in the shell structure is addressed. Analysis of single-particle energy shifts obtained with realistic and schematic interactions, as well as a rigorous spin-tensor decomposition of the TBME's, indicate an important role played by the central and tensor components of the nuclear interaction in the vanishing of $N = 20$, $N = 28$ shell closures in neutron-rich nuclei ($^{32}$Mg and $^{42}$Si and around) and creation of $N = 16$ magic number near $^{24}$O. The main signature of the tensor force is confirmed to be the characteristic behavior of spin-orbit partners (moving in opposite directions). However, the evolution of the gaps involving orbitals with different *nl* quantum numbers, as well as formation of shell gaps in heavy nuclei, requires more study.

# Acknowledgments

I am grateful to Faiçal Azaiez and the organizing committee of the International Joliot-Curie School for their invitation and for their patience during too extended delay of the present manuscript preparation. My special thanks to Kris Heyde (University of Ghent, Belgium), for many things I learned during the recent years of our collaboration, as well as for a careful reading of the present manuscript and numerous comments. I thank Etienne Caurier and Frédéric Nowacki (IPHC, Strasbourg, France) for introducing me into the shell-model world.

# References

[1] http://www.fys.uio.no/compphys/cp/software.html.

[2] A. Andreyev et al. *Nature*, 405:430, 2000.

[3] R. K. Bansal and J. B. French. *Phys. Lett.*, 11:145, 1964.

[4] M. Baranger. *Nucl. Phys.* **A**, 149:225, 1970.

[5] B. R. Barrett and M. W. Kirson. *Adv. Nucl. Phys.*, 6:219, 1973.

[6] M. Bender, K. Bennaceur, T. Duguet P.-H. Heenen, T. Lesinski, and J. Meyer. *Phys. Rev.* **C**, 80:064302, 2009.

[7] M. Bender, P.-H. Heenen, and P.-G. Reinhard. *Rev. Mod. Phys.*, 75:121, 2003.

[8] H. Bethe. *Ann. Rev. Nucl. Part. Sci.*, 21:93, 1971.

[9] S. K. Bogner, T. T. S. Kuo, and A. Schwenk. *Phys. Rep.*, 386:1, 2003.

[10] B. H. Brandow. *Rev. Mod. Phys.*, 39:771, 1967.

[11] J. Britz, A. Pape, and M. S. Anthony. *Atom. Data Nucl. Data Tables*, 69:125, 1998.

[12] B. A. Brown. *Prog. Part. Nucl. Phys.*, 47:517, 2001.

[13] B. A. Brown, A. Etchegoyen, W. D. M. Rae, N. S. Godwin, W. A. Richter, C. H. Zimmerman, W. E. Ormand, and J. S. Winfield. The computer code oxbash. *MSU-NSCL Report*, No. 524, 1984.

[14] B. A. Brown and W. A. Richter. *Phys. Rev.* **C**, 74:034315, 2006.

[15] B. A. Brown, W. A. Richter, and B. H. Wildenthal. *J. Phys. G*, 11:1191, 1985.

[16] B. A. Brown and B. H. Wildenthal. *Ann. Rev. Nucl. Part. Sci.*, 38:29, 1988.

[17] P. J. Brussaard and P. W. M. Glaudemans. *Shell-Model Applications in Nuclear Spectroscopy*. North-Holland, Amsterdam, 1977.

[18] E. Caurier, G. Martínez-Pinedo, F. Nowacki, A. Poves, and A. P. Zuker. The shell model as a unified view of nuclear structure. *Rev. Mod. Phys.*, 77:427, 2005.

[19] E. Caurier and F. Nowacki. *Acta Physica Polonica*, 30:705, 1999.

[20] E. Caurier, F. Nowacki, A. Poves, and J. Retamosa. *Phys. Rev.* **C**, 58:2033, 1998.

[21] S. Cohen and D. Kurath. *Nucl. Phys.*, 73:1, 1965.

[22] L. Coraggio, A. Covello, A. Gargano, N. Itaco, and T. T. S. Kuo. *Prog. Part. Nucl. Phys.*, 62:135, 2009.

[23] D. Dean, T. Engeland, M. Hjorth-Jensen, M. Kartamyshev, and E. Osnes. *Prog. Part. Nucl. Phys.*, 53:419, 2004.

[24] M. Dufour and A. P. Zuker. *Phys. Rev.* **C**, 54:1641, 1996.

[25] J. P. Elliott, A. D. Jackson, H. A. Mavromatis, E. A. Sanderson, and B. Singh. *Nucl. Phys.* **A**, 121:241, 1968.

[26] D. R. Entem and R. Machleidt. *Phys. Rev.* **C**, 68:041001, 2003.

[27] E. Epelbaum, W. Gloeckle, and U.-G. Meissner. *Nucl. Phys.* **A**, 747:362, 2005.

[28] A. L. Goodman. *Nucl. Phys.* **A**, 287:1, 1977.

[29] K. Heyde et al. *Phys. Rep.*, 102:291, 1983.

[30] K. Heyde, J. Jolie, J. Moreau, J. Ryckebusch, and M. Waroquier. *Nucl. Phys.* **A**, 466:189, 1987.

[31] K. Heyde and J. L.Woods. *J. Phys. G*, 17:135, 1991.

[32] Kris L. G. Heyde. *The Nuclear Shell Model*. Springer-Verlag, Heidelberg, second corrected and enlarged edition, 2004.

[33] M. Hjorth-Jensen, T. T. S. Kuo, and E. Osnes. *Phys. Rep.*, 261:125, 1995.

[34] M. Honma, T. Otsuka, B. A. Brown, and T. Mizusaki. *Phys. Rev.* **C**, 65:061301(R), 2002.

[35] M. Honma, T. Otsuka, B. A. Brown, and T. Mizusaki. *Phys. Rev.* **C**, 69:034335, 2004.

[36] J. Jaenecke. *Phys. Rep.*, 147:735, 1966.

[37] R. Julin, K. Helariutta, and M. Muikku. *J. Phys. G*, 27:R109, 2001.

[38] M. W. Kirson. *Phys. Lett. B*, 51:110, 1973.

[39] K. Klingenbeck et al. *Phys. Rev.* **C**, 15:1483, 1977.

[40] T. T. S. Kuo. *Ann. Rev. Nucl. Part. Sci.*, 24:101, 1974.

[41] T. T. S. Kuo and G. E. Brown. *Nuclear Physics*, 85:40, 1966.

[42] M. H. Macfarlane and J. B. French. *Rev. Mod. Phys.*, 32:567, 1960.

[43] G. Martínez-Pinedo, A. P. Zuker, A. Poves, and E. Caurier. *Phys. Rev.* **C**, 55:187, 1997.

[44] T. Mizusaki. *RIKEN Accel. Prog. Rep.*, 33:14, 2000.

[45] P. Navratil, S. Quaglioni, I. Stetcu, and B.R. Barrett. nucl-th/0904.0463.

[46] P. Navrtil, V. G. Gueorguiev, J.P. Vary, W.E. Ormand, and A. Nogga. *Phys. Rev. Lett.*, 99:042501, 2007.

[47] F. Nowacki. structure en couches des noyaux: de la stabilité à la limite d'existence. Ecole Joliot-Curie de Physique Nucléaire, 2002.

[48] F. Nowacki. *DESCRIPTION MICROSCOPIQUE DES PROCESSUS FAIBLES DANS LES NOYAUX SPHERIQUES*. PhD thesis, IReS, Strasbourg, 1996.

[49] F. Nowacki. *Acta Physica Polonica*, 38:1369, 2007.

[50] F. Nowacki and A. Poves. *Phys. Rev.* **C**, 79:014310, 2009.

[51] E. W. Ormand and C. W. Johnson. Redstick code, 2002.

[52] E. Osnes and D. Strottman. *Phys. Rev.* **C**, 45:662, 1992.

[53] T. Otsuka, R. Fujimoto, Y. Utsuno, B. A. Brown, M. Honma, and T. Mizusaki. *Phys. Rev. Lett.*, 87:082502, 2001.

[54] T. Otsuka, M. Honma, T. Mizusaki, et al. *Prog. Part. Nucl. Phys.*, 47:319, 2001.

[55] T. Otsuka, T. Suzuki, R. Fujimoto, H. Grawe, and Y. Akaishi. *Phys. Rev. Lett.*, 95:232502, 2005.

[56] S. C. Pieper. *Nucl. Phys.* **A**, 751:516, 2005.

[57] S. C. Pieper and R. B. Wiringa. *Ann. Rev. Nucl. Part. Sci.*, 51:53, 2001.

[58] A. Poves. Le modèle en couches. Ecole Joliot-Curie de Physique Nucléaire, 1997.

[59] A. Poves and A. P. Zuker. *Phys. Rep.*, 70:235, 1981.

[60] W. Satula, R. A. Wyss, and M. Zalewski. *Phys. Rev.* **C**, 78:011302, 2008.

[61] J. P. Schiffer and W. W. True. *Rev. Mod. Phys.*, 48:191, 1976.

[62] N. A. Smirnova, B. Bally, K. Heyde, F. Nowacki, and K. Sieja. *Phys. Lett. B*, 686:109, 2010.

[63] N. A. Smirnova, A. De Maesschalck, A. Van Dyck, and K. Heyde. *Phys. Rev.* **C**, 69:044306, 2004.

[64] N. A. Smirnova, A. De Maesschalck, and K. Heyde. *AIP Conf. Proc.*, 819:475, 2006.

[65] R. A. Sorensen. *Nucl. Phys.* **A**, 420:221, 1984.

[66] O. Sorlin and M.-G. Porquet. *Prog. Part. Nucl. Phys.*, 61:602, 2008.

[67] C. Thibault, R. Klapisch, C. Rigaud, A.M. Poskancer, R. Prieels, L. Lesard, and W. Reisdorf. *Phys. Rev.* **C**, 12:644, 1975.

[68] A. Umeya and K. Muto. *Phys. Rev.* **C**, 74:034330, 2006.

[69] M. Vallières and A. Novoselsky. *Nucl. Phys.* **A**, 570:345c, 1993.

[70] S. Weinberg. *Phys. Lett. B*, 251:288, 1990.

[71] E. P. Wigner. In W.O. Milligan, editor, *Proceedings of the Robert A. Welch Foundation Conference on Chemical Research*, volume 1, page 88. Welch Foundation, Houston, 1958.

[72] J. L. Wood et al. *Phys. Rep.*, 215:101, 1992.

[73] K. Yoro. *Nucl. Phys.* **A**, 333:67, 1980.

[74] M. Zalewski, W. Satula, J. Dobeczewski, P. Olbratowski, M. Rafalski, T.R. Werner, and R.A. Wyss. *Eur. Phys. J. A*, 42:577, 2009.

[75] A. P. Zuker and M. Dufour. nucl-th/9505012.